Journal of Nanobiotechnology

RESEARCH

Open Access

Mitochondria-targeted nanovesicles for ursodeoxycholic acid delivery to combat neurodegeneration by ameliorating mitochondrial dysfunction

Shizheng Zhang[1,2,3†], Mengmeng Li[4,5*†], Yuan Li[2,4,6†], Shike Yang[4,6,7†], Jian Wang[4,6], Xiaoxiang Ren[4], Xiuhui Wang[4], Long Bai[4], Jianping Huang[1,2,3], Zhen Geng[4*], Guosheng Han[8*], Yibin Fang[9*] and Jiacan Su[4,10*]

Abstract

Mitochondria are pivotal in sustaining oxidative balance and metabolic activity within neurons. It is well-established that mitochondrial dysfunction constitutes a fundamental pathogenic mechanism in neurodegeneration, especially in the context of Parkinson's disease (PD), this represents a promising target for therapeutic intervention. Ursodeoxycholic acid (UDCA), a clinical drug used for liver disease, possesses antioxidant and mitochondrial repair properties. Recently, it has gained attention as a potential therapeutic option for treating various neurodegenerative diseases. However, multiple barriers, including the blood-brain barrier (BBB) and cellular/mitochondrial membranes, significantly hinder the efficient delivery of therapeutic agents to the damaged neuronal mitochondria. Macrophage-derived nanovesicles (NVs), which can traverse the BBB in response to brain inflammation signals, have demonstrated promising tools for brain drug delivery. Nevertheless, natural nanovesicles inherently lack the ability to specifically target mitochondria. Herein, artificial NVs are loaded with UDCA and then functionalized with triphenylphosphonium (TPP) molecules, denoted as UDCA-NVs-TPP. These nanovesicles specifically accumulate in damaged neuronal mitochondria, reduce oxidative stress, and enhance ATP production by 42.62%, thereby alleviating neurotoxicity induced by 1-methyl-4-phenylpyridinium (MPP+). Furthermore, UDCA-loaded NVs modified with TPP successfully cross the BBB and accumulate in the striatum of PD mice.

Introduction

Neurodegeneration refers to the gradual deterioration of neuronal structure and function, which are the fundamental building blocks of the nervous system [1]. This decline can result in distinct pathological abnormalities within the central nervous system, collectively referred to as neurodegenerative diseases. Notable examples include Parkinson's disease (PD), Alzheimer's disease (AD), and Huntington's disease (HD) [2]. Despite various neurodegenerative diseases, there is broad consensus that mitochondrial involvement represents a key shared factor in these diseases [3].Mitochondria, as essential regulators of

†Shizheng Zhang, Mengmeng Li, Yuan Li and Shike Yang contributed equally to this work.

*Correspondence:
Mengmeng Li
mengmengli@shu.edu.cn
Zhen Geng
nanboshan1987@163.com
Guosheng Han
hgsxing72@tongji.edu.cn
Yibin Fang
fangyibin@163.com
Jiacan Su
drsujiacan@163.com

Full list of author information is available at the end of the article

© The Author(s) 2025. **Open Access** This article is licensed under a Creative Commons Attribution-NonCommercial-NoDerivatives 4.0 International License, which permits any non-commercial use, sharing, distribution and reproduction in any medium or format, as long as you give appropriate credit to the original author(s) and the source, provide a link to the Creative Commons licence, and indicate if you modified the licensed material. You do not have permission under this licence to share adapted material derived from this article or parts of it. The images or other third party material in this article are included in the article's Creative Commons licence, unless indicated otherwise in a credit line to the material. If material is not included in the article's Creative Commons licence and your intended use is not permitted by statutory regulation or exceeds the permitted use, you will need to obtain permission directly from the copyright holder. To view a copy of this licence, visit http://creativecommons.org/licenses/by-nc-nd/4.0/.

These nanoparticles significantly improve PD symptoms, as demonstrated by a 48.56% reduction in pole climb time, a 59.09% increase in hanging ability, and the restoration of tyrosine hydroxylase levels to normal, achieving remarkable therapeutic efficacy. Our work highlights the immense potential of these potent UDCA-loaded, mitochondria-targeting nanovesicles for efficient treatment of PD and other central neurodegenerative diseases.

Keywords Neurodegenerative diseases, UDCA, MNVs, Mitochondrial dysfunction, BBB, Mitochondrial targeting

cell survival and apoptosis, also play a crucial role in the process of aging. The onset and progression of neurodegenerative diseases are closely associated with early mitochondrial dysfunction [4].

PD is a well-known neurodegenerative disorder that primarily affects the nervous system, causing a gradual breakdown of specific brain regions responsible for motor control and other cognitive functions. Central to the pathology of PD is the progressive loss of dopaminergic neurons, particularly in the nigrostriatal system, a critical structure within the brain that plays a key role in regulating movement [5]. Currently, the main pharmacological treatments for PD include dopamine replacement therapies, dopamine receptor agonists and catabolic enzyme inhibitors, aimed at maintaining dopamine levels in the nigrostriatal system to alleviate Parkinson's symptoms [6, 7]. It's worth noting that these therapeutic approaches do not repair the damaged dopaminergic neurons nor reverse neuronal apoptosis. As dopaminergic neurons are lost during the progression of PD, the effectiveness of above drugs diminishes, accompanied by side effects such as motor fluctuations [8, 9].

Consequently, it is crucial to develop innovative treatments aimed at repair neurons for treating PD. Metabolic activity in active neurons in the brain requires substantial energy consumption. Mitochondria, as the primary site of ATP production, are crucial for distributing energy throughout neuronal cells, thereby regulating cell fate and maintaining tissue homeostasis [10]. Evidences indicates that dysfunction of these neuronal mitochondria can trigger the onset of PD [11]. Furthermore, mitochondrial respiratory chain dysfunction has been identified in brain tissue samples collected postmortem from individuals with PD [12]. Additionally, various neurotoxins, such as 1-methyl-4-phenyl-1,2,3,6-tetrahydropyridine(MPTP) [13] and rotenone [14], can disrupt neuronal mitochondrial function, leading to oxidative stress and autophagic defects in mitochondria. Therefore, neuronal mitochondria are emerging as promising therapeutic targets for PD. A key approach to improving mitochondrial dysfunction involves reducing oxidative stress through antioxidant mechanisms, as mitochondrial dysfunction may lead to excessive ROS, thereby causing severe inflammation and oxidative stress. Various antioxidants have been found to effectively reduce MPTP-induced neuronal apoptosis and mitochondrial dysfunction [15, 16].

Ursodeoxycholic acid (UDCA) is a clinically used drug with antioxidant properties that was initially developed for the treatment of liver diseases, it is currently being investigated for the treatment of neurodegenerative disorders. UDCA has the ability to prevent the buildup of reactive oxygen species, the disruption of mitochondrial membrane potential, and the depletion of ATP in neuronal cells, which may improve autophagic flux and alleviate cellular apoptosis [17]. Furthermore, UDCA has the ability to regulate mitochondrial activity, autophagic processes, and apoptosis in PD induced by MPTP/MPP, thereby safeguarding dopaminergic neurons from the detrimental effects of oxidative stress [18, 19]. However, the effectiveness of UDCA in accumulating within the brain and neuronal mitochondria is restricted by its limited capacity to cross the BBB and its low solubility in water, impeding the clinical development of UDCA as a potential therapeutic agent [20]. Therefore, there is an urgent need to develop delivery systems with excellent mitochondrial targeting capabilities to address mitochondrial dysfunction in neurons and improve PD treatment outcomes.

Macrophages, as immune cells, possess a natural capacity to respond to brain inflammation signals. Integrins existed on the macrophage membrane could interact with cell adhesion molecules located on the surface of brain endothelial cells, facilitating their natural passage across the BBB to reach inflammatory lesion areas [21]. Therefore, macrophage-derived nanovesicles (MNVs), especially artificial MNVs, are effective drug delivery platforms for crossing the BBB due to their simple preparation and preserved cellular membrane information [22, 23]. Despite the significant advantages shown by artificial MNVs in brain drugs delivery, they still lack mitochondrial targeting capabilities, thus preventing efficient accumulation of drugs in mitochondria. Mitochondria possess a distinctive feature of maintaining a high transmembrane potential across their inner membrane, which enables the selective attraction of positively charged molecules such as triphenylphosphonium (TPP) through electrostatic interactions [24]. Compared to other mitochondrial-targeting strategies, such as those based on mitochondrial lipid composition or specific signals, TPP offers a more efficient, versatile, and reliable approach for targeting mitochondria [25, 26].

Here, we have developed a mitochondria-targeting nanomedicine for PD therapy (Scheme 1). Specifically,

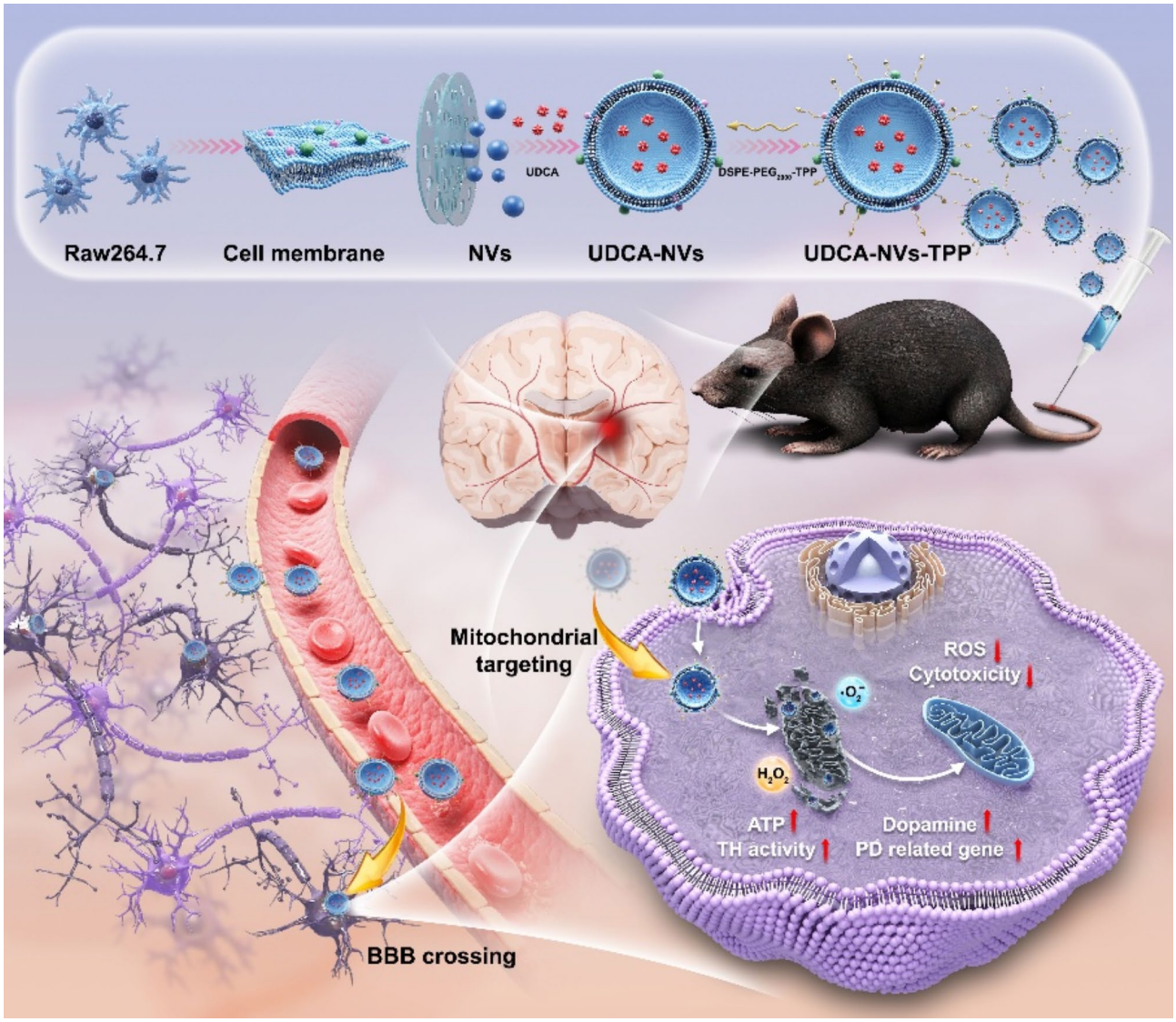

Scheme 1 Schematic diagram of research design and experimental process

by loading UDCA into artificial NVs and further modifying the NVs with the mitochondria-targeting molecule TPP, the resulting nanocomplex UDCA-NVs-TPP can effectively traverse the BBB and target damaged neuronal mitochondria. The nanoparticles exhibit excellent antioxidative properties, ameliorate the ROS levels and oxidative stress status of mitochondria in MPP^+-damaged SH-SY5Y neuronal cells, enhance ATP production, thereby restoring mitochondrial dysfunction, and reducing apoptosis in damaged cells. Moreover, the UDCA-NVs-TPP nanoparticles could traverse the BBB, enhancing the enrichment of UDCA-loaded vesicles within the brain. Additionally, the mitochondria-targeted nanoparticles significantly increased the activity of tyrosine hydroxylase in the striatum system of PD mice, markedly upregulated mitochondrial metabolism, dopamine metabolism, and the expression levels of genes closely associated with PD. This led to improvements in limb grip strength, limb coordination, and a reduction in the motor sluggishness symptoms of Parkinsonian mice. Our research demonstrates that mitochondrial-targeted nanovesicles loaded with UDCA exhibit significant advantages in crossing the BBB, alleviating mitochondrial oxidative stress, and reducing mitochondria-mediated neuronal apoptosis, thereby exerting a potent and effective therapeutic effect in the neurodegenerative disease.

Results and discussion

Preparation and characterization of UDCA-NVs-TPP NPs

Artificial nanovesicles (NVs) from macrophage were generated by disrupting RAW264.7 cells using an ultrasonic cell disruptor. This process resulted in the formation of nanoscale cellular fragments, which can be subsequently membrane-treated and rearranged to form nanovesicles

(Fig. 1a) [27, 28]. The concentration of the obtained NVs was quantified using the BCA assay, which measured the protein concentration at 2.52 mg/ml (Figure S1). The NVs loaded with UDCA (abbreviated as UDCA-NVs) were prepared in an aqueous solution using ultrasound conditions, following a previously reported method [29]. Various amounts of UDCA (0.5, 1.5, 2.0, 2.5, 3.5 mg) were attempted to be incorporated into 2.5 mg of NVs. The encapsulation (EE) and UDCA-loading efficiency (LE) of UDCA-NVs were assessed via HPLC. The highest encapsulation efficiency (79.49%) was achieved with the smallest amount of UDCA loading (0.5 mg), while the highest loading efficiency (31.76%) occurred when the amount of UDCA was 2.5 mg. As EE decreased and LE increased with higher UDCA loads, a balance was sought. Consequently, the 2.5 mg UDCA loading condition, which offered a good compromise between LE and EE, was selected for further experiments (Fig. 1b and Figure S2). Compared to existing exosome-based drug delivery systems, which require complex separation and purification steps and are often cost-prohibitive, the nanoplatform based on artificial nanovesicles offers superior drug loading efficiency and a simpler preparation process [29, 30]. The optimized UDCA-NVs were further modified with DSPE-PEG_{2000}-TPP (abbreviated as UDCA-NVs-TPP) to enhance their mitochondrial targeting ability. The resulting UDCA-NVs-TPP nanoparticles are designed to reach inflammatory neurons and specifically target mitochondria to improve their mitochondrial biogenesis. At different time points (4 h, 8 h, 12 h, 24 h), the retention rates of UDCA in UDCA-NVs-TPP decreased from 72.39 to 56.81%, demonstrating that encapsulation by NVs, along with DSPE-PEG2000-TPP modification, presented excellent stability (Figure S3). Notably, a previous study demonstrated that macrophage-derived exosomes loaded with catalase (Exo-CAT), prepared using the sonication method, exhibited similar stability, further confirming the superior loading

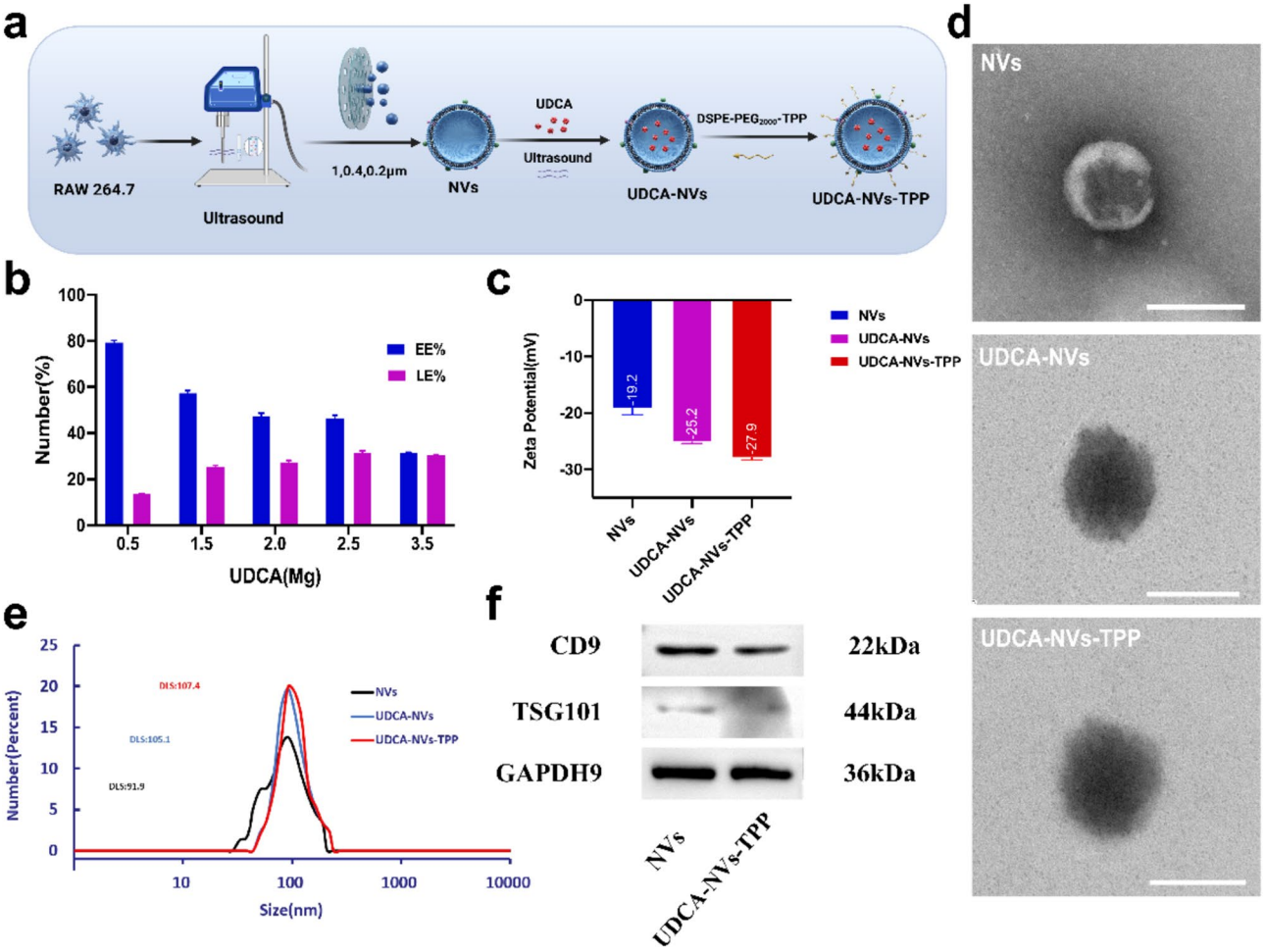

Fig. 1 Synthesis and characterization of NVs, UDCA-NVs, and UDCA-NVs-TPP. **a**) Schematic diagram of the preparation of NVs, loading of UDCA into NVs to form UDCA-NVs, and modification of UDCA-NVs with DSPE-PEG2000-TPP to form UDCA-NVs-TPP. **b**) EE and LE of NVs for various dosages of UDCA. **c**) Zeta potential of NVs, UDCA-NVs, and UDCA-NVs-TPP. **d**) TEM images of NVs, UDCA-NVs, and UDCA-NVs-TPP, scale bar = 100 nm. **e**) Hydrodynamic sizes of NVs, UDCA-NVs, and UDCA-NVs-TPP. f) Verification of labeled proteins in NVs and UDCA-NVs-TPP by protein imprinting

efficiency and stability of nanovesicles produced via this approach [29]. Furthermore, the surface charge of NVs with and without modification was determined using the Malvern Zetasizer, revealing a zeta potential of -19.2 mV for NVs (Fig. 1c). The drug loading and modification increased zeta potential of surface, which is comparable to that of endogenously released vesicles [31]. Transmission Electron Microscopy (TEM) was employed to depict the morphology and size of all groups to characterizing their size distribution. NVs demonstrated a liposomal bilayer structure with a circular shape, exhibiting localized invaginations, and measuring approximately 100 nm in size (Fig. 1d). However, after loaded with UDCA, the vesicles observed under TEM appeared darker, which can be attributed to the abundant internal drug substances obstructing the passage of electron beams (Figure S4). Additionally, Dynamic Light Scattering (DLS) analysis revealed that the vesicle size distribution in solution primarily ranged from 32.7 to 200 nm, with an average size of 91.97 nm (Fig. 1e). These findings are consistent with the TEM results and align with the size range commonly reported for exosomes [32]. Additionally, western blotting was used to determine the effects of UDCA loading and DSPE-PEG2000-TPP modification on artificial NVs derived from macrophage. The obtained results showed that the characteristic proteins CD9 and TSG101 from the macrophage membrane were still present in UDCA-NVs-TPP (Fig. 1f). As is well-established, CD9 and TSG101 are membrane-associated proteins on macrophage [33, 34]. These proteins were found to be preserved in the nanovesicles even after drug loading and modification, indicating that the processing method of mitochondria-targeted biomimetic nanoplatform could retain the integrity of the macrophage membrane.

The targeting characteristics of UDCA-NVs-TPP NPs towards neuronal cell mitochondria

Next, the biocompatibility and mitochondria targeting of UDCA-NVs-TPP was evaluated using SH-SY5Y cell (Fig. 2a). The results showed that the viability of SH-SY5Y cells did not significantly decrease with increasing concentrations of UDCA-NVs-TPP (Fig. 2b), demonstrating the excellent biocompatibility of UDCA-NVs-TPP nanoparticles. The neurotoxin MPP + can inhibit the activity of mitochondrial complex I in SH-SY5Y cells, leading to reduced ATP production and increased oxidative stress, thereby inducing oxidative damage and apoptosis of cells. The results showed that 3 mM MPP^+ significantly reduced cell viability (Fig. 2c), thus this concentration was chosen to establish an inflammatory SH-SY5Y cell model for in vitro experiments with nanomedicines. Moreover, to further evaluate the protective effects and determine the optimal concentration of UDCA-NVs-TPP on MPP^+-treated SH-SY5Y cells, the CCK-8 assay results demonstrated that a concentration of 31.25 μM UDCA-NVs-TPP provided significant protection (Fig. 2d). Therefore, this concentration of nanovesicles was chosen for subsequent in vitro experiments. As shown in Fig. 2e, g, after treatment with MPP^+, SH-SY5Y cells exhibited significantly higher uptake of UDCA-NVs-TPP compared to UDCA-NVs at 2 h, and the uptake of both reached a similar amount after 4 h of incubation. This could be attributed to the saturation of nanoparticle uptake by the cells. To further investigate the ability of UDCA-NVs-TPP to target neuronal cell mitochondria, we labeled nanovesicles with FITC and stained mitochondria in SH-SY5Y cells with a mitochondrial red probe. After incubating nanovesicles with MPP^+-treated SH-SY5Y cells for 4 h, we observed higher accumulation of UDCA-NVs-TPP in mitochondrial regions of SH-SY5Y cells compared to the UDCA-NVs group, as indicated by green fluorescence intensity (Fig. 2f, h). To further validate the effective accumulation of the therapeutic agent, SH-SY5Y cells incubated with nanovesicle groups for 2 and 4 h were harvested, subjected to cell lysis, and subsequently processed for mitochondrial isolation via differential centrifugation. The UDCA content within the mitochondria of SH-SY5Y cells incubated with UDCA-NVs-TPP was significantly higher than that in the UDCA-NVs group (Figure S5). These results demonstrate that UDCA-loaded nanovesicles with TPP modification exhibit enhanced mitochondrial targeting capability, consistent with previous studies [35]. These results suggest that UDCA-NVs-TPP can be rapidly taken up by neuronal cells and targeted to mitochondrial regions, a process attributed to the presence of the positively charged TPP, which is drawn to mitochondria via electrostatic forces due to their high transmembrane potential [24].

UDCA-NVs-TPP NPs scavenge oxidative stress to protect neuronal mitochondria

After the protective effects of TPP-modified UDCA-loaded nanovesicles on neuronal cells and their mitochondrial targeting ability were confirmed, the oxidative scavenging capacity and the subsequent repair effects of UDCA-NVs-TPP on damaged mitochondria were examined (Fig. 3a). Firstly, the antioxidant capacity of various concentrations of UDCA-NVs-TPP was evaluated via ABTS assay, the results confirmed the UDCA-NVs-TPP possessed the antioxidant activity in a concentration-dependent manner (Fig. 3b). Since the primary function of mitochondria is to produce ATP and maintain cellular energy, we then examined the impact of UDCA-NVs-TPP on mitochondrial ATP production in MPP^+-treated cells. As illustrated in Fig. 3c, MPP^+ significantly decreased ATP production in SH-SY5Y cells, likely due to the disruption of the mitochondrial respiratory chain [36–38]. Notably, UDCA-NVs-TPP effectively

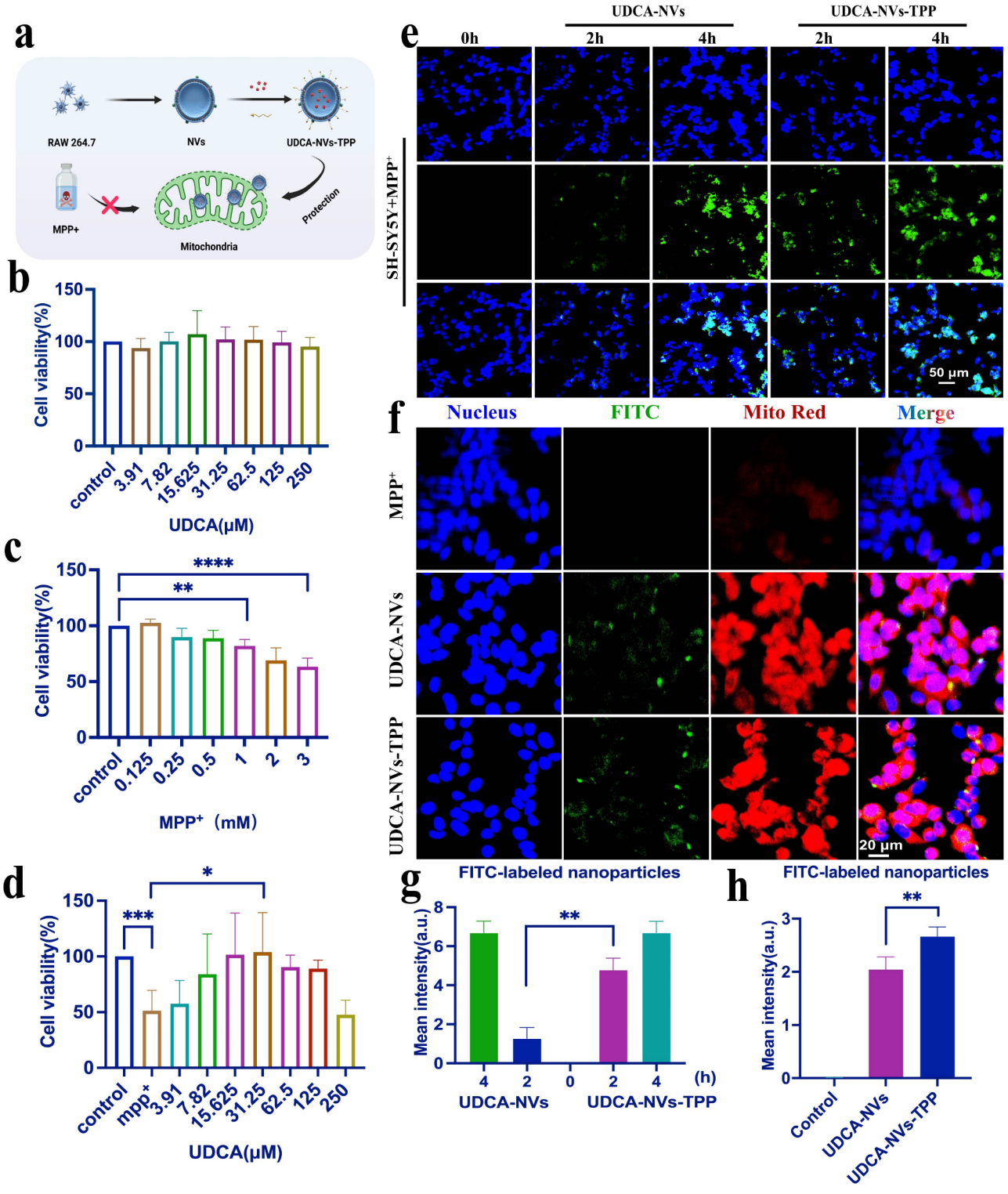

Fig. 2 Characterization of UDCA-NVs-TPP and assessment of its extracellular targeting capability towards neurons. **a**) A schematic illustration depicting the preparation of UDCA-NVs-TPP and its targeted delivery to the mitochondria of neuronal cells. **b**) Cell viability of SH-SY5Y cells following treatment with UDCA-NVs-TPP ($n=4$). **c**) Cell viability of SH-SY5Y cells after exposure to MPP^+ ($n=4$). **d**) Assessment of SH-SY5Y cell viability following pretreatment with UDCA-NVs-TPP, followed by exposure to 3 mM MPP^+ ($n=4$). **e**) Observation of the internalization of SH-SY5Y cells with UDCA-NVs and UDCA-NVs-TPP at 2 h and 4 h using confocal microscopy. Blue indicates cell nuclei; green represents TITC-labeled UDCA-NVs-TPP. **f**) Utilizing confocal laser scanning microscope (CLSM) to assess the targeting capability of UDCA-NVs and UDCA-NVs-TPP on mitochondria in SH-SY5Y cells. Blue represents cell nuclei; green signifies FITC-labeled UDCA-NVs and UDCA-NVs-TPP; red denotes mitochondria. **g**) Quantitative analysis of FITC-labeled nanoparticles ($n=3$). **h**) Quantitative analysis of FITC-labeled nanoparticles ($n=4$)

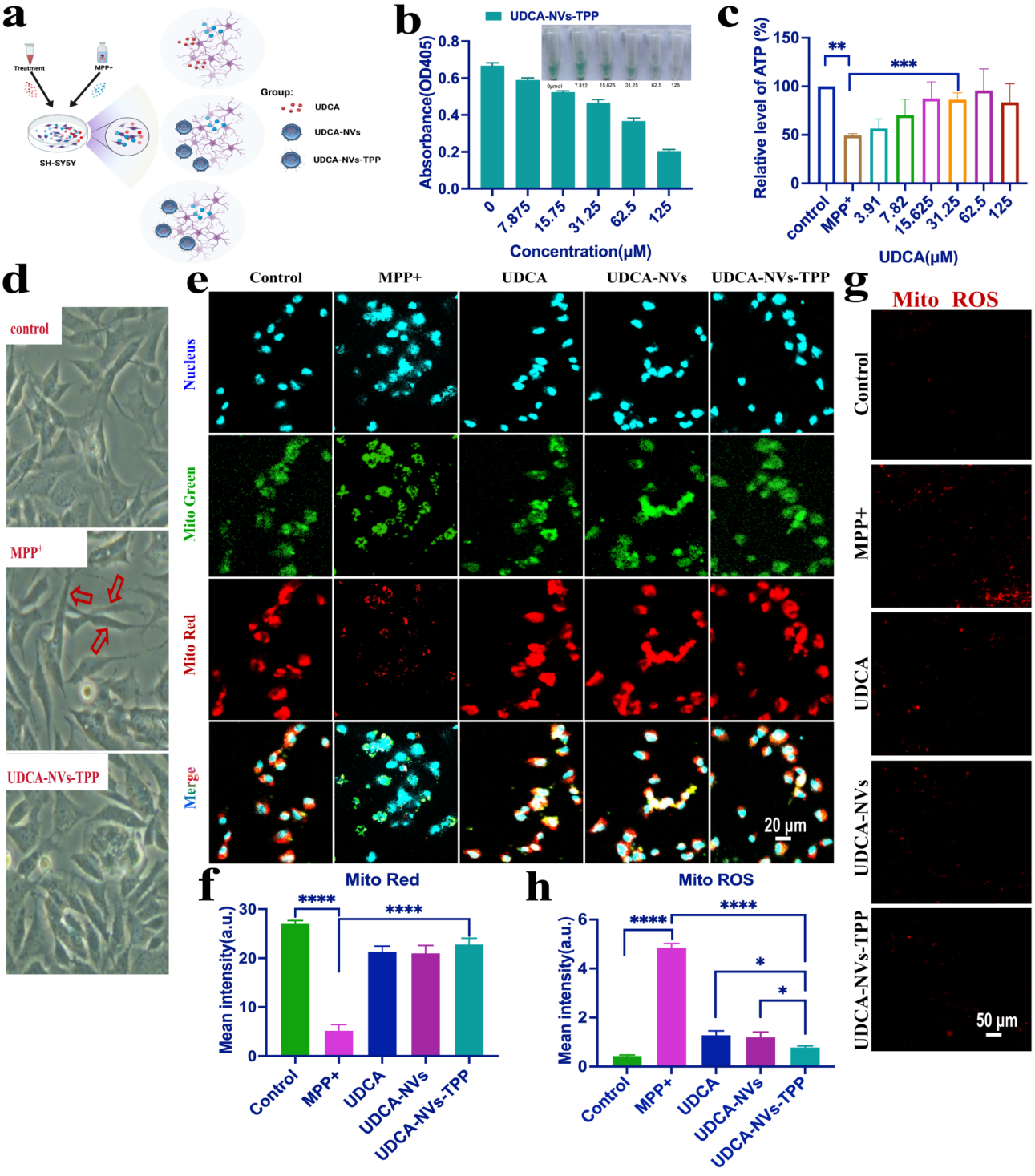

Fig. 3 Protective and reparative effects of UDCA-NVs-TPP on SH-SY5Y against mitochondrial damage induced by MPP^+. **a**) Schematic representation of different treatment groups. **b**) Overall antioxidative capacity of UDCA-NVs-TPP accompanied by images of the solutions ($n=3$). **c**) Measurement of ATP levels in SH-SY5Y cells pretreated with UDCA-NVs-TPP and subsequently exposed to MPP^+ ($n=3$). **d**) Representative morphological images of SH-SY5Y cells: cells exposed to MPP^+, cells pretreated with UDCA-NVs-TPP and then exposed to MPP^+, captured using an inverted microscope. **e**) CLSM images demonstrate that SH-SY5Y cell mitochondria pretreated with UDCA-NVs-TPP are intact and highly active. Blue: cell nuclei; green: total mitochondria; red: active mitochondria. **f**) Quantitative assessment of active mitochondria ($n=3$). **g**) CLSM images demonstrate the levels of mitochondrial ROS produced by SH-SY5Y cells after pretreatment with UDCA, UDCA-NVs, UDCA-NVs-TPP, followed by co-incubation with MPP^+ for 24 h. Red: mitochondrial ROS. h) Quantitative analysis of mitochondrial ROS levels ($n=3$)

improves mitochondrial ATP production by 42.62%, protecting them from neurotoxin-induced damage in a concentration-dependent manner. Significant protection was observed at 31.25μM, consistent with the previously mentioned protective effects of UDCA-NVs-TPP on cells. Additonally, the protection effect of UDCA-NVs-TPP can be observed under microscope. As shown in Fig. 3d, UDCA-NVs-TPP transformed the slender, rod-shaped morphology of MPP^+-treated SH-SY5Y cells into a more typical multipolar or polygonal shape. At the mitochondrial level, we further assessed the differences and variations in both the quantity and activity of mitochondria following treatment with various groups, using two distinct probes. The green fluorescence represents total mitochondria, while the red fluorescence indicates active mitochondria. The merged orange fluorescence reflects the proportion of active mitochondria. As illustrated in Fig. 3e, untreated SH-SY5Y cells exhibit higher levels of active mitochondria and total mitochondrial content. Upon combination, orange-red fluorescence is observed around the blue nuclei, indicating higher proportions of active mitochondria and total mitochondrial content. In contrast, the group treated solely with MPP^+ shows lower red fluorescence signals, indicating a lower proportion of active mitochondria. Earlier reports have pointed out that MPP^+ disrupts the mitochondrial electron transport chain, generating excessive reactive oxygen species (ROS), thus causing mitochondrial damage [39, 40]. Importantly, experimental groups treated with UDCA, UDCA-NVs, and UDCA-NVs-TPP significantly enhanced mitochondrial activity in SH-SY5Y subjected to MPP^+ exposure, with UDCA-NVs-TPP showing the most pronounced effect, approaching levels of mitochondrial activity seen in normal cells (Fig. 3f). This suggests its superiority in protecting cellular mitochondria from MPP^+ damage. Following pretreatment with UDCA, UDCA-NVs, and UDCA-NVs-TPP for 2 h, the red fluorescence emitted by ·OH markers in cellular mitochondria significantly decreased, with UDCA-NVs-TPP showing the most pronounced difference, comparable to fluorescence intensity observed in normal cells (Fig. 3g, h). These results indicate that mitochondria-targeted UDCA-loaded nanovesicles (UDCA-NVs-TPP) can significantly reduce excessive mitochondrial ROS production induced by MPP^+, thereby protecting SH-SY5Y cells.

Targeting ability of UDCA-NVs-TPP NPs in vitro and vivo

The above experiments demonstrate that UDCA-NVs-TPP can target neuronal mitochondria in inflammatory environments, improving mitochondrial biogenesis. While, for the PD, crossing the BBB is a primary requirement for effective drug treatment. Macrophages are known for their unique inflammation tropism. They are able to efficiently cross the BBB by interacting with ICAM-1. Additionally, they exhibit neuronal targeting ability through the interaction between integrins and VCAM-1 [41, 42]. Therefore, the ability of TPP-modified UDCA-loaded artificial nanovesicles to cross the BBB was verified both in vitro and in vivo.

Mouse brain endothelial cells (bEnd3) were used as a BBB model in vitro. They were cultured in transwell inserts with a 0.4 μm pore size to form a tight monolayer. Different groups of nanovesicles labeled with FITC fluorescence were used. After incubation for 1, 3, and 6 h in the in vitro model, it was observed that macrophage-derived artificial NVs could penetrate the tight endothelial cell layer. As shown in Fig. 4a, the transendothelial crossing rates of all nanovesicle (NV)-based groups increased over time. At 6 h, the crossing rate for UDCA-NVs-TPP was 58.04%. Notably, the incorporation of UDCA and the modification with TPP targeting ligands did not significantly alter the ability of these nanovesicles to traverse the endothelial cell layer, which is consistent with previous studies [43]. Macrophage-derived nanovesicles have been shown to cross the BBB by interacting with adhesion molecules on the endothelial cell surface [44]. Among these interactions, intercellular adhesion molecule-1 (ICAM-1) has been identified as a key mediator facilitating the passage of nanovesicles across the barrier [45]. To further verify the role of ICAM-1 in the transport of UDCA-NVs-TPP, we pretreated bEnd3 cells with an anti-ICAM-1 antibody (Figure S6). Upon blocking ICAM-1 with anti-ICAM-1 antibodies, the crossing rates of NVs, UDCA-NVs, and UDCA-NVs-TPP were significantly reduced (Fig. 4a and Figure 7). Specifically, after 6 h, the crossing rates decreased to 34.37%, 36.01%, and 34.89%, respectively. In contrast, without anti-ICAM-1 pre-treatment, the crossing rates remained higher, at 61.92%, 58.60%, and 58.04% for NVs, UDCA-NVs, and UDCA-NVs-TPP, respectively. This significant reduction in crossing rates upon ICAM-1 blockade underscores the critical role of ICAM-1 in facilitating the transendothelial transport of these nanovesicles. Next, live animal and ex vivo imaging were used to evaluate the in vivo brain accumulation of UDCA-loaded NVs, both with and without TPP modification. The distribution of Dir-labeled UDCA-NVs and UDCA-NVs-TPP in brain tissue was captured at various time points following injection into mice (Fig. 4b, c, d). We observed fluorescence signals of UDCA-NVs and UDCA-NVs-TPP nanovesicles in the mouse brain 0.5 h post-injection, which gradually accumulated in brain tissue over time, peaking between 4 and 10 h. Notably, the incorporation of TPP into UDCA-loaded NVs significantly enhanced brain accumulation, with increases of 107% at 4 h and 96% at 6 h compared to UDCA-loaded NVs without modification. This enhanced accumulation is likely due to the electrostatic interactions between the positively

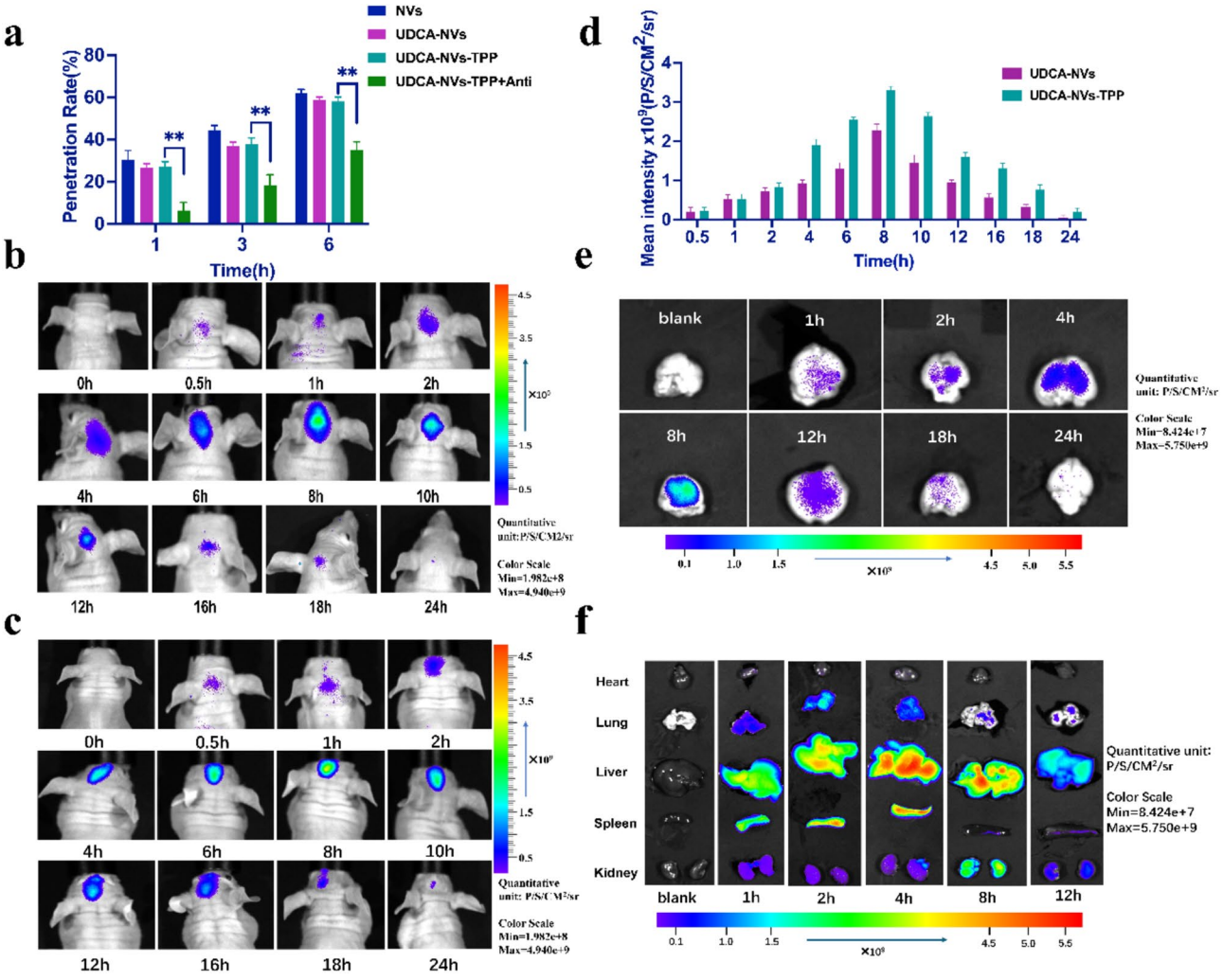

Fig. 4 Evaluation of the ability of UDCA-NVs-TPP to cross the BBB in vitro and in vivo, and its distribution in major organs. **a**) Permeability across the in vitro BBB of NVs, UDCA-NVs, and UDCA-NVs-TPP ($n = 3$). **b**) In vivo fluorescence imaging of nude mice, following intravenous injection of Dir-labeled UDCA-NVs, was conducted over a 0–24 h period. **c**) In vivo fluorescence imaging was performed on nude mice after intravenous injection of Dir-labeled UDCA-NVs-TPP, with observations taken over a 0–24 h period. **d**) Fluorescence quantification of Dir-labeled UDCA-NVs-TPP and UDCA-NVs in nude mice after intravenous injection for 0–24 h ($n = 3$). **e**) Ex vivo fluorescence imaging of brain tissues after ex vivo intravenous injection of Dir-labeled UDCA-NVs-TPP for 0–24 h. **f**) Ex vivo fluorescence imaging of organs after intravenous injection of Dir-labeled UDCA-NVs-TPP for 0–12 h

charged TPP molecules and the cellular/mitochondrial membranes. Subsequently, fluorescence intensity began to decline, becoming nearly undetectable by 24 h, indicating complete metabolism within the cranial cavity. The live imaging revealed stronger fluorescence intensity of UDCA-NVs-TPP particles in brain regions (Fig. 4d), indicating that TPP modification enhances the accumulation of nanoparticles in the brain, likely due to faster cellular uptake of TPP-modified nanovesicles, as shown in Fig. 2e. Furthermore, fluorescence imaging analysis of brain tissues isolated at various time points revealed the retention of UDCA-NVs-TPP within the brain (Fig. 4e), with half-life and peak accumulation results consistent with those observed in live imaging. However, fluorescence intensity in ex vivo brain tissues (Figure S8) was weaker compared to live imaging, possibly due to the circulation of UDCA-NVs-TPP in the systemic system. Additionally, fluorescence intensity analysis of heart, lung, liver, spleen, and kidney tissues at different time points revealed the distribution of UDCA-NVs-TPP in various organs. The highest accumulation of UDCA-NVs-TPP was observed in the liver, followed by the kidneys, indicating that its metabolism primarily occurs in the hepatic system. Fluorescence intensity began to diminish in all tissues by 12 h (Fig. 4f). These results suggest that UDCA-loaded nanovesicles with mitochondrial targeting exhibit superior brain accumulation in vivo, effectively crossing the BBB. The enhanced brain localization, confirmed by both live and ex vivo imaging, indicates their potential for treating neurodegenerative diseases. This

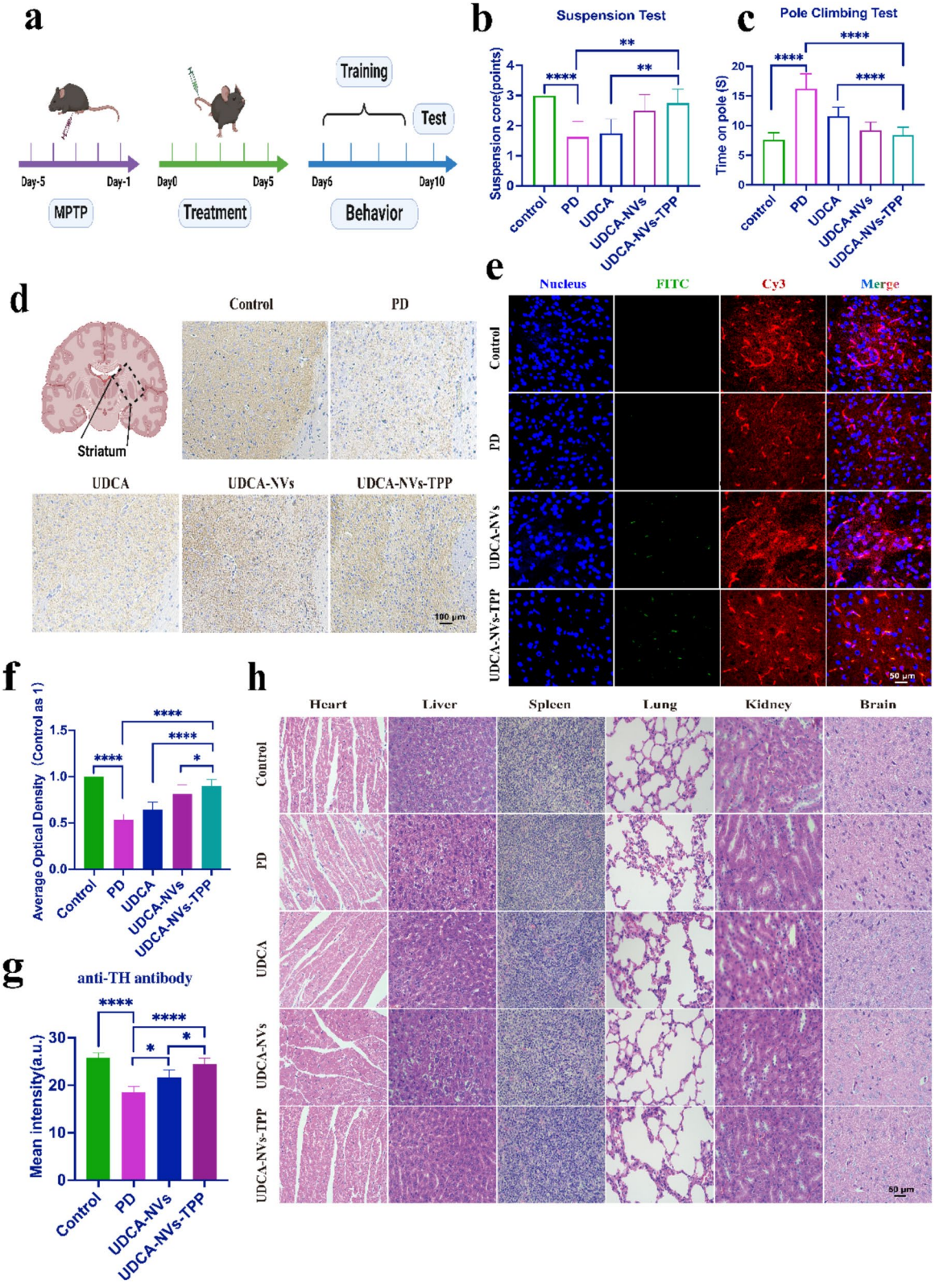

Fig. 5 (See legend on next page.)

(See figure on previous page.)

Fig. 5 Treatment of PD mice with UDCA-NVs-TPP. **a**) A schematic diagram depicting the treatment of PD mice with UDCA-NVs-TPP, as well as behavioral testing and related experimental procedures conducted on the mice. **b**) Suspension Test of mice in Control group, PD group, UDCA group, UDCA-NVs group, and UDCA-NVs-TPP group ($n = 3$). **c**) Pole Climbing Test conducted on mice from Control group, PD group, UDCA group, UDCA-NVs group, and UDCA-NVs-TPP group ($n = 3$). **d**) Immunoreactivity of TH in the striatum was assessed in mice from the Control, PD, UDCA, UDCA-NVs, and UDCA-NVs-TPP groups ($n = 3$). **e**) CLSM images showing TH immunofluorescence in the striatum were obtained from mice in the Control, PD, UDCA-NVs, and UDCA-NVs-TPP groups, along with CLSM images of FITC-labeled UDCA-NVs and UDCA-NVs-TPP in the striatum; Blue: cell nuclei; green: FITC-labeled nanoparticles; red: TH-positive neurons. **f**) Quantitative analysis of TH immunoreactivity in the striatum of mice ($n = 3$). **g**) Quantitative analysis of Cy3-labeled anti-TH antibody. **h**) H&E staining was performed on the major organs to evaluate the biocompatibility of nanoparticles ($n = 3$)

targeting capability, combined with efficient mitochondrial delivery, underscores the therapeutic advantage of these nanovesicles.

Evaluation of UDCA-NVs-TPP NPs therapy in MPTP-Induced PD mice

To evaluate the potential therapeutic effects of UDCA-NVs-TPP, a PD mouse model was created using MPTP induction. Following treatment, the mice underwent behavioral assessments to determine the impact of the therapy on motor functions [46]. (Fig. 5a). The mice were randomly assigned to five groups ($n = 8$ per group), including C57BL/6J mice as normal controls (Control group), untreated Parkinson's disease mice (PD group), and PD mice that received intravenous injections of UDCA at a dosage of 5 mg/kg, PD mice intravenously injected with UDCA-NVs, and PD mice intravenously injected with UDCA-NVs-TPP. As is well known, the motor symptoms of PD typically encompass resting tremors and disturbances in postural balance. We conducted pole climbing and hanging tests on each group of mice, which rely on limb grip strength, manipulation of limb turning, and coordination during climbing. These tests can assess the animals' motor coordination and bradykinesia. In the hanging test, mice in the PD group exhibited significantly lower scores compared to those in the control group. The scores of mice in the UDCA-NVs and UDCA-NVs-TPP groups were notably higher than those in both the PD and UDCA groups. (Fig. 5b). It was observed that mice in the PD group were found to take considerably longer to descend from the top to the bottom of the pole, in contrast to the untreated normal group. The total climbing time of Parkinsonian mice treated with consecutive 5-day injections of UDCA-NVs and UDCA-NVs-TPP was significantly reduced compared to both the PD group and the UDCA treatment group, with times approaching those of the normal control group (Fig. 5c). The above results demonstrate that UDCA-loaded NVs can improve motor symptoms in a PD mouse model.

Furthermore, the therapeutic impact of UDCA-NVs-TPP on PD mice was examined at the protein level. Tyrosine hydroxylase (TH) is the rate-limiting enzyme in dopamine synthesis within brain tissue. Alterations in TH expression levels in the striatum of individuals with PD provide a direct indication of the extent of dopamine neuron repair and their overall quantity [47, 48]. Immunohistochemical staining and analysis of the striatal tissue of mice after 5 days of drug injection showed that TH levels in the UDCA-NVs-TPP group were notably higher compared to those in the other treatment groups, including UDCA-NVs and UDCA, and even approached levels seen in the Ctrl group (Fig. 5d, f). These findings suggest that UDCA-NVs-TPP effectively repairs MPTP-induced damage to mouse striatum, maintaining high levels of TH expression.

Moreover, FITC-labeled UDCA-NVs-TPP and UDCA-NVs particles were used to investigate the targeting of TPP-modified nanovesicles in the striatum tissue of mice and their effect on TH expression. After 5 days of treatment injection, immunofluorescence staining was performed to localize the vesicular drugs in the striatal tissue and assess the surrounding levels of TH. The green fluorescence signal from UDCA-NVs-TPP in the striatum tissue of mice was observed to be more intense than that from UDCA-NVs, as observed through fluorescence microscopy (Fig. 5e and S9). Positively stained TH labeled with Cy3 exhibited red fluorescence, with significantly higher intensity observed in the UDCA-NVs-TPP group compared to other treatment groups (Fig. 5e, g), consistent with the results shown in Fig. 5d. These results indicate that UDCA-NVs-TPP effectively targets the mitochondria of dopaminergic neurons in the striatum of PD mice and restores damaged tyrosine hydroxylase activity. Additionally, Major organs (such as brain, heart, liver, spleen, lungs, and kidneys) were harvested from five groups of mice and subsequently stained with hematoxylin and eosin (HE) to assess the biocompatibility of TPP-modified nanovesicles. (Fig. 5h). No notable histopathological abnormalities were detected in the tissues of any of the mice. Moreover, the NVs-based nanoplatform did not trigger any inflammatory responses, as evidenced by the maintenance of white blood cell (WBC), lymphocyte (LYM), monocyte (MON), and neutrophil (N) counts within normal ranges. Similarly, no abnormalities were observed in red blood cell (RBC) counts or platelet levels, both of which are indicative of normal hematopoiesis and coagulation function. Additionally, biomarkers associated with liver (ALT, AST, ALB) and kidney (BUN, UA, CREA) function did not show any significant alterations across the experimental groups (Figure S10 and Figure S11). Collectively, these results

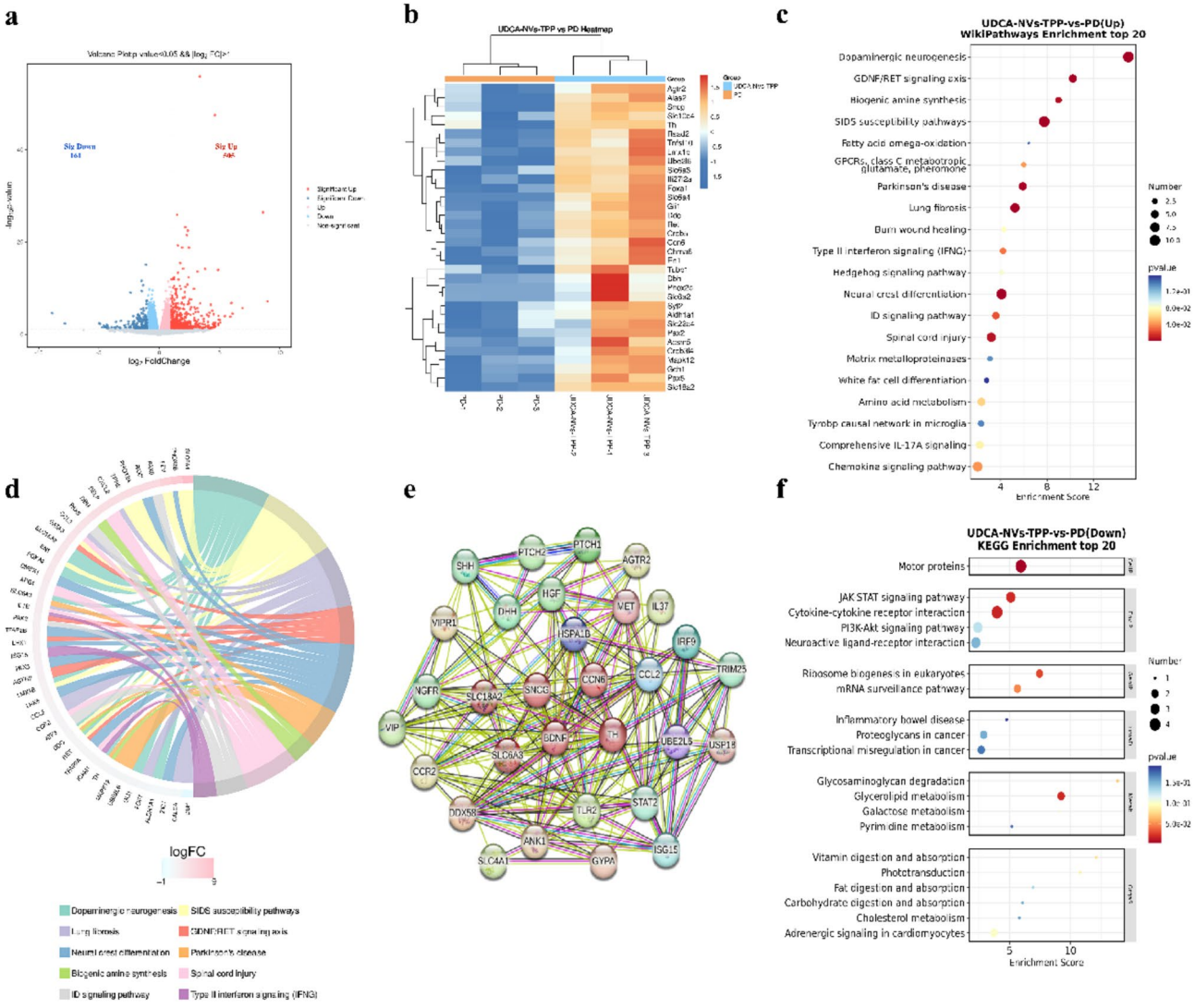

Fig. 6 Transcriptome sequencing of the striatum in PD mice was treated with UDCA-NVs-TPP. **a**) volcano plot of DEGs between the PD and UDCA-NVs-TPP group. **b**) Heatmap analysis was conducted to compare DEGs between the PD and UDCA-NVs-TPP group. **c**) Bubble plot of the top 20 enriched WikiPathways for upregulated DEGs between the PD and UDCA-NVs-TPP group. **d**) Chord diagram of the top 10 enriched WikiPathways for overall DEGs between the PD and UDCA-NVs-TPP group. **e**) Protein–protein interaction (PPI) networks associated with key signaling pathways. **f**) Bubble plot of the top 20 enriched KEGG pathways for downregulated DEGs between the PD and UDCA-NVs-TPP group

suggest that UDCA-NVs-TPP administration does not induce organ toxicity or systemic inflammation. The above results suggest that mitochondria-targeted UDCA-loaded nanovesicles (UDCA-NVs-TPP) effectively target the striatum in PD mice, enhancing tyrosine hydroxylase levels and improving motor function. The data demonstrate the superior therapeutic potential of UDCA-NVs-TPP in repairing MPTP-induced damage, with excellent biocompatibility and safety, making them a promising treatment strategy for PD.

Transcriptome sequencing and data analysis

To explore the therapeutic potential of mitochondria-targeted artificial vesicles loaded with ursodeoxycholic acid in the PD mouse, we conducted mRNA transcriptome sequencing of the striatum in both the UDCA-NVs-TPP group and the PD group (Fig. 6). The analysis revealed significant gene expression changes, with 505 genes showing upregulation and 161 genes exhibiting downregulation in the UDCA-NVs-TPP group when compared to the PD group (q-value < 0.05 and |log2FC| > 1) (Fig. 6a).

We also identified specific DEGs related to mitochondrial repair and dopamine metabolism that were significantly upregulated in the UDCA-NVs-TPP group (q-value < 0.05 and 0.6 < |log2FC| < 1). These include genes such as Alas2, Rsad2, Tnfsf10 (related to mitochondrial metabolism), and Agtr2, Sncg, Slc10a4, Lmx1b, Slc6a4, Ifi27l2a, Ddc, Mapk12, Slc18a2, Slc6a3, Th

(associated with dopamine metabolism and PD) (Fig. 6b). These findings suggest that UDCA-loaded nanovesicles affect mitochondrial levels and upregulate dopamine metabolism in the striatum of Parkinsonian mice, alleviating PD.

To understand the biological implications of these differentially expressed genes (DEGs), we performed enrichment analysis. Gene Ontology (GO) analysis indicated that UDCA-NVs-TPP treatment significantly impacted cellular components and molecular functions related to dopaminergic synapses, neuronal projections, transcription regulatory complexes, and chemokine activity (Figure S12).Moreover, pathway enrichment analysis using WikiPathways revealed that UDCA-NVs-TPP treatment significantly upregulated pathways involved in dopaminergic neurogenesis, biogenic amine synthesis, and PD (Fig. 6c, d), suggesting that these mitochondria-targeted nanovesicles positively influence the generation and function of dopaminergic neurons in the striatum [49].

Notably, the enrichment of the GDNF/RET signaling axis in the transcriptomic data implies that UDCA-NVs-TPP may promote neurotrophic factor signaling [50, 51], thereby supporting the survival and function of dopaminergic neurons, a key aspect in the PD therapy. Additionally, the observed enrichment in neural crest differentiation pathways may reflect the potential of UDCA-NVs-TPP to contribute to broader neurodevelopmental and repair processes [52]. These analyses highlight the significant impact of mitochondria-targeted artificial vesicles loaded with ursodeoxycholic acid on the functional repair of the neural system in PD mice.

The Protein-Protein Interaction (PPI) analysis was employed to identify key proteins involved in the maintenance of dopaminergic neurons and mitochondrial function (Fig. 6e). The PPI network revealed several crucial protein-coding gene, including TH, CCN6, BDNF, SNCG, SLC18A2, and SLC6A3, which play significant roles in the mitochondrial electron transport chain and respiratory complexes [53, 54], as well as the development of dopaminergic neurons. These genes are involved in processes such as axonal structure regulation [55, 56], synaptic activity maintenance, and the regulation of dopamine transporter activity [57, 58], facilitating the sodium- and chloride-dependent transport of dopamine [59, 60]and promoting the conversion of tyrosine to dopamine [61].

Furthermore, KEGG pathway analysis revealed a prominent downregulation of the JAK-STAT signaling pathway (Fig. 3f, Figure S13). Abnormal activation of this pathway is known to be triggered by oxidative stress and neuroinflammation in the early stages of Parkinson's disease [62]. Specifically, cytokines such as IL-6 and TNF-α activate JAK kinases, which in turn phosphorylate STAT proteins, leading to their translocation to the nucleus and initiating downstream gene transcription [63, 64]. Therefore, the observed downregulation of the JAK/STAT pathway following UDCA-NVs-TPP treatment may be attributed to its antioxidant and mitochondrial repair properties, consistent with previous findings [65, 66].

Conclusion

This study developed a novel nanodrug delivery system based on artificial nanovesicles designed to effectively deliver UDCA into neuronal mitochondria for the treatment of PD. Compared to synthetic nanoparticles [67, 68], the macrophage-derived nanovesicles stand out due to their naturally BBB penetration ability, biocompatibility, prolonging systemic circulation [69]. The incorporation of TPP further enhanced the system's ability to deliver therapeutic agents directly to neuronal mitochondria, addressing a critical challenge in PD treatment. Our findings revealed that UDCA-NVs-TPP accumulates efficiently within neuronal mitochondria, significantly improving mitochondrial function by reducing oxidative stress, lowering ROS levels, and promoting ATP production. In the PD mouse model, intravenous administration of UDCA-NVs-TPP led to marked improvements in motor function, including enhanced grip strength, limb coordination. Furthermore, the treatment significantly increased the levels and activity of TH in the striatum, a key enzyme involved in dopamine synthesis, thereby contributing to the regeneration of dopaminergic neurons and the alleviation of PD symptoms. Overall, this study highlights the potential of mitochondria-targeted UDCA-loaded nanovesicles as a promising therapeutic strategy for neurodegenerative diseases like Parkinson's. The data underscore the advantages of using macrophage-derived nanovesicles modified with functional ligands as effective carriers for lipophilic drugs, offering a novel approach to the design of intravenous nanosystems targeting mitochondrial dysfunction in the treatment of PD.

It's worth noting that UDCA-NVs-TPP may also have potential therapeutic effects for other neurodegenerative diseases due to their common therapeutic target and barriers. Mitochondrial dysfunction constitutes a fundamental pathogenic mechanism in various neurodegeneration, thus present a common target for therapeutic intervention [3, 4]. Moreover, the therapeutic agents for mitochondrial repair should traverse the blood-brain barrier and cellular/mitochondrial membranes [2, 70]. In this study, the mitochondria-targeted biomimetic nanoplatform has demonstrated its ability to overcome above multiple biological barriers, thereby enabling the efficient delivery of therapeutic agents to damaged neuronal mitochondria. Therefore, this nanoplatform holds significant potential for the treatment of other neurodegenerative diseases.

Despite the aforementioned advantages, mitochondria-targeted biomimetic nanoplatforms face challenges related to large-scale production and potential immunogenicity. The development of standardized protocols is essential for achieving large-scale production and ensuring reproducibility. Future studies should prioritize conducting comprehensive immunogenicity profiling to facilitate clinical translation. Additionally, the therapeutic effects of this nanoplatform for other neurodegenerative disorders, such as Alzheimer's and Huntington's diseases, where mitochondrial dysfunction is implicated, merits further exploration.

Experimental section

Preparation of NVs、UDCA-NVs、UDCA-NVs-TPP

Mouse mononuclear macrophage leukemia cells(RAW264.7)were cultured in a 10 cm dish to 80% density, digested, and centrifuged to obtain a single cell suspension. Subsequently, using an ultrasonic cell disruptor (JY96-IIN, SCIENTZ, CHINA) in a mode of 20–25 kHz, 1 s on, 1.5 s off, with a frequency of 65%, for a total of 15 min. Following this, the disrupted cell suspension was sequentially extruded through 1 μM (Cat. no.10418704, Whatman), 0.4 μM (Cat.no.10417104, Whatman), and 0.2 μM (Cat.no.10417004, Whatman) polycarbonate membrane filters using a small-scale cell extruder for 5 consecutive passes each [71–73]. The extruded suspension mentioned above was further separated and purified using a high-speed freezing centrifuge (Fresco 21, Thermo Fisher Scientific, Germany). The centrifuge was set to operate at 4 °C with a speed of 2000 g for 15 min to pellet the cell debris, and the supernatant was subsequently collected. Subsequently, the supernatant was then subjected to a second centrifugation at 4 °C with a speed of 20,000 g for 15 min. After discarding the supernatant, the precipitated macrophage vesicles were gently resuspended using a sterile DPBS solution to ensure uniform dispersion. Finally, the vesicles were stored at -80 °C for future use, and the macrophage-derived artificial vesicles obtained were defined as NVs. UDCA was encapsulated into NVs using ultrasonication [29]. Initially, a certain amount of NVs was mixed with a UDCA solution (Cat. no. U820345, Macklin) and placed in an ice bath. Ultrasonication (500 V, 2.0–2.5 kHz, 6% P) for 15 min resulted in the successful synthesis of UDCA-NVs. After resuspending 2.5 mg of UDCA-NVs in 4 ml of DPBS solution, 2.5 mg of DSPE-PEG2000-TPP was added for co-incubation and mixed stirring to facilitate their binding [74]. Subsequently, centrifugation at 20,000 g for 15 min in a centrifuge yielded the precipitate, resulting in UDCA-NVs modified with DSPE-PEG2000-TPP, designated as UDCA-NVs-TPP.

Characterization: The images of NVs, UDCA NVS and UDCA NVS TPP were obtained by TEM (ht7800), and the DLS and zeta potential of the above particles were measured by Malvern Zetasizer nano zs90.

Western blotting analysis

NVs and UDCA-NVs-TPP were lysed with RIPA lysis buffer (Cat. no. P0013D, Beyotime) to release proteins. The proteins from the lysed samples were loaded onto polyacrylamide gels (Cat.no. 800013290, Sinopharm Chemical Reagent Co., Ltd) according to predetermined concentrations. The protein samples were subjected to gel electrophoresis for analysis. (Cat.no. #S8010-500 g, Solarbio). The gel concentration voltage was set at 80 V and the separation gel voltage at 130 V. Electrophoresis was stopped when the bands reached the bottom of the glass plate. Subsequently, the isolated protein was transferred to a specific membrane (PVDF) (Cat.no. IPVH00010, MILLIPORE). The PVDF membrane from the previous step was placed in a suitable 5% skim milk solution and incubated on a shaker (TY-80 A/S, Changzhou Runhua Electric Appliance Co., Ltd, CHINA) for 1 h for blocking. The primary antibody for the target protein was appropriately diluted with antibody dilution buffer, and the blocked PVDF membrane was placed in a hybridization bag. The membrane was washed five times with TBST. The secondary antibody was then diluted to the appropriate concentration using 5% skim milk. Incubate the membrane with the secondary antibody for 1 h and add electrochemiluminescence. Adjust exposure conditions based on different intensities of light and analyze the results accordingly.

The EE% and LE%

UDCA solutions containing 0.5, 1.0, 1.5, 2.0, 2.5 and 3.5 mg were separately added to a suspension of 2.5 mg NVs for drug loading under ultrasonication. After ultrasonication, the solution was centrifuged at 20,000 g for 15 min in a centrifuge, and the precipitate was collected as UDCA-NVs, while the supernatant contained excess UDCA. The supernatant was subjected to HPLC (LC-20 A, SHIMADZU, Japan) to quantify the UDCA content [75]. Finally, EE% and LE% were calculated using the following formulas.

$$LE\% = \frac{W_{total} - W_{free}}{M_{total}} \times 100\%$$

W_{total} refers to the initial added total amount of UDCA, W_{free} refers to the content of UDCA in the supernatant, and M_{total} refers to the total amount of UDCA-NVs.

Stability assessment of UDCA-NVs-TPP

To evaluate the stability of UDCA-NVs-TPP, UDCA-NVs-TPP at a concentration of 2.5 mg/ml were incubated in 2 ml PBS at 37 °C in the dark. At various time points

(4, 8, 12, 24 h), the supernatant was collected and filtered, and the UDCA content was measured using HPLC. The UDCA content retained in UDCA-NVs-TPP at each time point was determined by deducting the mass of UDCA present in the supernatant collected at different time points from the initial amount of UDCA.

Assessment of the antioxidant capacity of UDCA-NVs-TPP

The antioxidant capacity of UDCA-NVs-TPP was evaluated using ABTS (Cat. no. S0121, Beyotime) [76]. In brief, varying concentrations of UDCA-NVs-TPP (0, 3.91, 7.82, 15.625, 31.25, 62.5, 125, and 250 μM) were dispensed into a 96-well plate. Then working solution was added to UDCA-NVs-TPP, then the absorbance was recorded by spectrophotometer (perkinlemer enspire, Singapore).

Assessment of the uptake capability of UDCA-NVs-TPP by neuron cells

UDCA-NVs and UDCA-NVs-TPP were labeled with the FITC (Cat.no. A70075, Innochem) to track their distribution within SH-SY5Y cells at various time intervals. The cells were plated on coverslips at the bottom of 12-well culture plates. Following a 24-hour incubation with 3 mM MPP^+, FITC-labeled UDCA-NVs and UDCA-NVs-TPP were added and incubated for 2 h and 4 h, respectively. Obtaining fluorescence image of cells with CLSM (FV1200, Olympus, Japan).

Equal volumes of UDCA-NVs and UDCA-NVs-TPP were added to SH-SY5Y cells and cultured for 2 and 4 h, respectively. At the designated time points, SH-SY5Y cells were collected for lysis, and mitochondria were isolated by differential centrifugation. Finally, the UDCA content in the mitochondria was quantified using HPLC.

Assessment of the targeting ability of UDCA-NVs-TPP to neuronal mitochondria in vitro

FITC-labeled UDCA-NVs and UDCA-NVs-TPP were used to track their distribution in mitochondria of SH-SY5Y cells at various time points. The cells were incubated with 3 mM MPP^+ for 24 h, followed by addition of FITC-labeled UDCA-NVs and UDCA-NVs-TPP, cultured separately for 4 h. Subsequently, incubation was conducted at incubator for 30 min together with 1 ml of MitoTracker Red CMXRos (Cat.no.C1049B, Beyotime). Fluorescence images were acquired using CLSM (excitation: 495 nm, 579 nm, 405 nm; emission: 520 nm, 599 nm, 461 nm, respectively).

Assay of cell toxicity

SH-SY5Y cells were cultured in SH-SY5Y specific medium for 24 h (Cat.no. h187-001b, iCell). Following the cells successfully adhered, they were exposed to various concentrations of UDCA-NVs-TPP (0, 3.91, 7.82, 15.625, 31.25, 62.5, 125, 250 μM) and different concentrations of MPP^+ (0.125, 0.25, 0.5, 1, 2, 3 mM) for 24 h. Subsequently, CCK-8 solution (Enhanced Cell Counting Kit-8, Cat. no. C0043, Beyontime) were added to the cells. The absorbance was recorded using a microplate reader. (BIOTEK, USA).

The relative cell viabilities were calculated using the following formula:

$$Cell\ viability\,(\%) = \frac{A\,(\text{sample}) - A\,(\text{blank})}{A\,(\text{control}) - A\,(\text{blank})} \times 100\%$$

Where:

- A(sample) is the mean absorbance of the treated cells.
- A(control) is the mean absorbance of untreated cells.
- A(blank) is the mean absorbance of the blank solution.

To assess the protective effects of UDCA-NVs-TPP, SH-SY5Y cells were initially treated with varying concentrations of UDCA-NVs-TPP and subsequently incubated with 3 mM MPP^+. Cell morphology was observed under inverted microscope (Olympus, Japan) in Ctrl, MPP^+ and UDCA-NVS-TPP group.

Detection of ATP content

We used the CellTiter-Glo Luminescent Cell Viability Assay Kit (CTL) (Cat. No. C0068M, Beyotime) to measure the ATP content in the cells. In essence, SH-SY5Y cells were exposed to different concentrations of UDCA-NVs-TPP (0, 3.91, 7.82, 15.625, 31.25, 62.5, 125 μM), then co-incubated with 3 mM MPP^+. Following this, 100μL CTL was added to the above cells, and finally subjected to luminescence measurements using a multi-mode microplate reader (PerkinElmer EnSpire, Singapore).

Measurement of intracellular mitochondrial ROS

We monitored the generation of mitochondrial hydroxyl radicals (·OH) using the CellMeter Mitochondrial Hydroxyl Radical Detection Assay Kit (MitoROS580, Cat. no. 16052, AAt Bioquest). SH-SY5Y cells were separately treated with UDCA (31.25μM), UDCA-NVs (31.25μM), and UDCA-NVs-TPP (31.25μM) for 2 h, followed by co-incubation with 3mM MPP^+. We added 1 ml of prepared 1x MitoROS580 working solution to the cells and then incubated them for 10 min. Subsequently, the fluorescent images were captured using a CLSM (excitation: 510 nm, emission:580 nm).

Staining of total and active mitochondria in cells

SH-SY5Y cells were respectively treated with UDCA, UDAC-NVs, and UDAC-NVs-TPP, each at a concentration of 31.25 μm, for 2 h. Subsequently, they were

co-incubated with 3 mM MPP^+ in a 37 °C incubator for 24 h. The SH-SY5Y cells were then co-incubated with 1 ml of MitoTracker Red CMXRos(Cat. No. C1049B, Beyotime). Subsequently, they were incubated with 1 ml of MitoTracker Green working solution (Cat. no. S26555μg, Shanghai Yuanye Bio-Technology Co., Ltd). Use 10 μg/mL Hoechst33342 (Cat. no. S19116, Shanghai Yuanye Bio-Technology Co., Ltd) to stain the cell nuclei. Fluorescence images are acquired using CLSM (excitation: 579, 490, 352 nm, emission: 599, 516, 454 nm, respectively).

The protective effects of UDCA-NVs-TPP on PD

To explore the protective and therapeutic effects of UDCA-NVs-TPP in vivo, a PD mouse model was created using 1-methyl-4-phenyl-1,2,3,6-tetrahydropyridine (MPTP) as the inducer [77], wherein MPTP was administered intraperitoneally at a dose of 30 mg/kg for 5 days, followed by subsequent drug treatment, behavioral tests, and relevant ex vivo experiments. The mice were randomly assigned to five groups ($n = 8$ each), namely (1) normal mice (Ctrl group), (2) PD mice with no treatment (PD group), (3) PD mice treated with UDCA via tail vein (UDCA group), (4) PD mice injected with UDCA-NVs via tail vein (5 mg kg^{-1}) (UDCA-NVs group), and (5) PD mice treated with UDCA-NVs-TPP via tail vein (5 mg kg^{-1}) (UDCA-NVs-TPP group). We selected a dosage of 5 mg/kg based on the delivery efficiency of our drug delivery system and previous studies [78, 79]. The mice used in the above groups were all male C57BL/6J mice aged 10–12 weeks.

Evaluation of UDCA-NVs-TPP crossing the BBB

We used immortalized mouse brain endothelial cells (bEnd3) as a model of the BBB to investigate the ability of UDCA-NVs-TPP to cross the BBB [80–82]. Initially, bEnd3 cells (5×10^4 cells/cm2) were cultured on the upper layer of transwell chambers (Cat.no.3412, Corning Life Sciences) with a pore size of 0.4μM for 48 h until a confluent monolayer with a transendothelial electrical resistance > 300Ω was established. Subsequently, equal amounts of FITC-labeled NVs, UDCA-NVs, and UDCA-NVs-TPP were added to different chambers and co-incubated with the cells at 37 °C, 5% CO2 for 1, 3, and 6 h. Fluorescence intensity was then measured at 1, 3, and 6 h using a fluorescence microplate reader (Ex: 485 nm, Em: 528 nm; BIOTEK Instruments, Winooski, VT, USA). The BBB penetration rate was assessed by calculating the relative fluorescence ratio (RFR, %), which is the ratio of the fluorescence intensity measured in the lower chamber to the initial fluorescence intensity added to the upper chamber, for NVs, UDCA-NVs, and UDCA-NVs-TPP. To further investigate the role of ICAM-1 in this process, we pretreated bEnd3 cells with anti-ICAM-1 antibodies (Cat.no.GB11106-50, Wuhan Sevier Bio Co., Ltd) and subsequently measured the BBB penetration rates of NVs, UDCA-NVs, and UDCA-NVs-TPP to assess the impact of antibody blockade on the transport of UDCA-NVs-TPP.

To investigate the ability of UDCA-NVs-TPP to cross the BBB and target brain tissues in vivo, UDCA-NVs and UDCA-NVs-TPP were intravenously injected into male BALB/c nude mice, aged 6–8 weeks. after being labeled with DiR (Cat.no. Y18318, Shanghai Yuanye Bio-Technology Co., Ltd), at a dose of 10 mg/kg. A multimodal in vivo imaging system (BLT-AniView100, Guangzhou Bolten Instrument Co., Ltd.) was used to acquire near-infrared fluorescence images at various time intervals, enabling the assessment of the distribution and accumulation of UDCA-NVs and UDCA-NVs-TPP throughout the body and in the brain. We further euthanized nude mice injected with DiR-labeled UDCA-NVs-TPP at different time points and dissected brain tissues to obtain intact ex vivo brain tissues. Subsequently, near-infrared fluorescence images were obtained using the aforementioned imaging system to quantify the intensity of fluorescence at different time points. Additionally, we investigated the accumulation of UDCA-NVs-TPP at different time points in the heart, lungs, liver, spleen, and kidneys.

Pole climbing test

In the center of a mouse housing cage, a wooden rod wrapped with gauze is firmly placed vertically. Subsequently, the experimental mice are positioned at the top of the pole, with their heads directed towards its end. The mice then instinctively turn around and rapidly descend to return to their familiar housing cage [83, 84]. The time taken by the mice to descend the entire length of the pole is recorded.

Suspension test

The experimental mice were suspended by their front paws on a horizontal wire, and instinctively, they grasped the wire with their hind limbs [85]. If a mouse could grip the wire with both hind limbs, it received a score of 3 points; if it grasped the wire with only one hind limb, it was awarded 2 points; if neither hind limb could grip the wire, it was scored 1 point. Finally, the scores were calculated and analyzed.

TH immunohistochemistry

Immunohistochemistry was employed to evaluate the expression levels of TH in the striatum. Firstly, dissect the brains of mice from each group (Ctrl, PD, UDCA, UDCA-NVs, UDCA-NVs-TPP group) to obtain the striatal tissues and then fix them on slides. Next, the striatal tissues on the slides will undergo protein fixation and permeabilization treatment, followed by the addition of Recombinant Anti-TH antibody (Mouse mAb) (Cat.

no. GB15181-100, Wuhan Servicebio Technology Co., Ltd). Subsequently, the second antibody labeled with fluorescence was added to specifically bind with the first antibody. Staining substrate was added for color development, and finally, the color reactions of the samples were observed to evaluate the expression level and activity of TH in the striatum. To further quantify the expression levels and activity, we obtained the Integrated Optical Density (IOD) values of the detected samples' images using ImageJ software (version 1.54f, America).

Immunofluorescence of TH

To investigate the restorative effect of UDCA-NVs-TPP on TH activity in the MPTP-induced striatal damage and its potential to target dopaminergic neurons, mice were grouped and subjected to different treatment regimens: (I) Healthy mice (Ctrl group); (II) Mice with MPTP-induced PD (PD group); (III) Mice with MPTP-induced PD received tail vein injection of FITC-labeled UDCA-NVs for 5 days (UDCA-NVs group); and (IV) Mice with MPTP-induced PD received tail vein injection of FITC-labeled UDCA-NVs-TPP for 5 days (UDCA-NVs-TPP group). After completing the above experiments, the striatum of mice was dissected for observation. Immunofluorescent staining for TH was performed on the striatum of mice from each group, and the intensity of the fluorescence was quantitatively analyzed, to assess the capability of UDCA-NVs-TPP in restoring TH activity in the striatum. To analyze the enrichment of TH in the striatum, labeled FITC UDCA-NVs and UDCA-NVs-TPP were utilized to evaluate their ability to target dopaminergic neurons.

H&E staining

H&E staining was applied to the major organs (such as brain, heart, liver, spleen, lungs, and kidneys) to assess the biocompatibility of UDCA-NVs-TPP.

Hematological and biochemical analysis

Blood was collected from mice in each group using sterile techniques and placed in EDTA-coated tubes for complete blood count (CBC) analysis. Serum was separated for liver and kidney function analysis.

RNA sequencing and analysis

Total RNA was isolated from the striatum of mice in the PD and UDCA-NVs-TPP groups ($n = 4$) using TRIzol reagent (Invitrogen, CA, USA). RNA purity and concentration were measured with a NanoDrop 2000 spectrophotometer (Thermo Fisher Scientific). The construction of transcription library, followed by transcriptional sequencing and analysis were carried out by OE Biotech Co. Ltd (Shanghai, China). mRNA sequencing analysis consisted of two main steps: RNA sequencing and analysis of differentially expressed genes (DEGs). The libraries were sequenced using the Illumina Novaseq 6000 platform, producing paired-end reads of 150 bp, with an average of approximately 26,655 raw reads per sample. The fastq formatted raw reads were processed using fastp1 to eliminate low-quality reads, resulting in approximately 22,519 clean reads per sample [86]. Alignment of these clean reads to the rat genome was performed using HISAT2 [87]. FPKM values for each gene were counted, and read counts were obtained with HTSeq-count [88]. DEGs analysis was conducted using DESeq2 [89], with DEGs identified based on a Q value threshold of < 0.05 and a fold change greater than 2 or less than 0.5. Hierarchical clustering analysis was conducted using R (version 3.2.0) to reveal gene expression patterns among different groups and samples. The R package ggradar was utilized to visualize radar plots showing the top 30 upregulated or downregulated DEGs. Enrichment analysis was conducted using the hypergeometric distribution algorithm to assess GO, Reactome, WikiPathway and KEGG pathways to identify significantly enriched terms in DEGs. Similarly, Column chart, chord diagrams, and bubble charts were generated using R (version 3.2.0) to illustrate significantly enriched terms. Gene set enrichment analysis was conducted using GSEA software, ranking predefined gene sets based on the degree of differential expression between the two sample types. This analysis determines the ranking order of the predefined gene set.

Statistical analysis

The data were analyzed by GraphPad Prism version 10.2.0 (GraphPad Software, San Diego, CA, USA). Results are presented as mean ± SD and were analyzed using one-way analysis of variance (ANOVA), then Tukey's post-hoc test for group comparisons. Significance was determined based on the following thresholds: $^{*}p < 0.05$, $^{**}p < 0.01$, $^{***}p < 0.001$, and $^{****}p < 0.0001$.

Supplementary Information

The online version contains supplementary material available at https://doi.org/10.1186/s12951-025-03258-5 .

Supplementary Material 1

Acknowledgements

Not applicable.

Author contributions

S.Z.Z.: Writing– original draft, Methodology, Investigation, Formal analysis, Data curation, Conceptualization. M.M.L.: Writing– review & editing, Visualization, Conceptualization, Supervision, Funding acquisition. Y.L.: Methodology, Investigation, Formal analysis. S.K.Y.: Methodology, Investigation, Formal analysis. J.W.: Methodology, Investigation. X.X.R.: Methodology, Investigation, Formal analysis. X.H.W.: Validation, Software. L.B.: Validation, Supervision, Conceptualization. J.H.: Validation, Supervision, Conceptualization. Z.G.: Validation, Supervision, Conceptualization. G.S.H: Methodology,

Conceptualization. Y.B.F.: Methodology. J.C.S.: Writing-review & editing, Supervision, Resources, Funding acquisition, Conceptualization.

Funding
The work was financially supported by the National Natural Science Foundation of China (82230071, 82172098, 32471395, 82472156), the Shanghai Committee of Science and Technology (23141900600), and the Natural Science Foundation of Shanghai (22ZR1423400). Natural Science Foundation of Fujian Province (2024J08122).

Data availability
Data is provided within the manuscript or supplementary information files.

Declarations

Ethics approval and consent to participate
All experimental involving animals were approved by the Experimental Animal Ethics Committee of the Shanghai University, Shanghai, People's Republic of China. The experiments followed the ethical care and handling guidelines for laboratory animals established by the National Institutes of Health (NIH).

Consent for publication
Not applicable.

Competing interests
The authors declare no competing interests.

Author details
[1]Department of Neurology, Wenzhou Central Hospital, Wenzhou 325000, China
[2]The Second Affiliated Hospital of Shanghai University, Wenzhou 325000, China
[3]Panvascular Disease Management Center, Wenzhou Central Hospital, Wenzhou 325000, China
[4]Institute of Translational Medicine, Shanghai University, Shanghai 200444, China
[5]Sanming Institute of Translational Medicine, Fujian 365004, China
[6]School of Medicine, Shanghai University, Shanghai 200444, China
[7]Department of Anesthesiology, Shanghai Zhongye Hospital, Shanghai 200941, China
[8]Department of Neurosurgery, Shanghai Fourth People's Hospital, School of Medicine, Tongji University, Shanghai 200434, China
[9]Stroke Center, Shanghai Fourth People's Hospital, School of Medicine, Tongji University, Shanghai 200434, China
[10]Department of Orthopedics, Xinhua Hospital, Shanghai Jiao Tong University School of Medicine, Shanghai 200092, China

Received: 12 December 2024 / Accepted: 20 February 2025
Published online: 11 March 2025

References

1. Mukherjee S, Madamsetty VS, Bhattacharya D, Roy Chowdhury S, Paul MK, Mukherjee A. Recent advancements of nanomedicine in neurodegenerative disorders theranostics. Adv Funct Mater. 2020;30(35):2003054.
2. Cavalli A, Bolognesi ML, Minarini A, Rosini M, Tumiatti V, Recanatini M, Melchiorre C. Multi-target-directed ligands to combat neurodegenerative diseases. J Med Chem. 2008;51(3):347–72.
3. Lin MT, Beal MF. Mitochondrial dysfunction and oxidative stress in neurodegenerative diseases. Nature. 2006;443(7113):787–95.
4. Itoh K, Nakamura K, Iijima M, Sesaki H. Mitochondrial dynamics in neurodegeneration. Trends Cell Biol. 2013;23(2):64–71.
5. Goldman SJ, Taylor R, Zhang Y, Jin S. Autophagy and the degradation of mitochondria. Mitochondrion. 2010;10(4):309–15.
6. Bloem BR, Okun MS, Klein C. Parkinson's disease. Lancet. 2021;397(10291):2284–303.
7. Armstrong MJ, Okun MS. Diagnosis and treatment of Parkinson disease: A review. JAMA. 2020;323(6):548–60.
8. Fahn S, Oakes D, Shoulson I, Kieburtz K, Rudolph A, Lang A, Olanow CW, Tanner C, Marek K. Levodopa and the progression of Parkinson's disease. N Engl J Med. 2004;351(24):2498–508.
9. Fabbrini G, Brotchie JM, Grandas F, Nomoto M, Goetz CG. Levodopa-induced dyskinesias. Mov Disorders: Official J Mov Disorder Soc. 2007;22(10):1379–89.
10. Tandler B, Hoppel CL, Mears JA. Morphological pathways of mitochondrial division. Antioxid (Basel) 2018, 7(2).
11. González-Rodríguez P, Zampese E, Stout KA, Guzman JN, Ilijic E, Yang B, Tkatch T, Stavarache MA, Wokosin DL, Gao L, et al. Disruption of mitochondrial complex I induces progressive parkinsonism. Nature. 2021;599(7886):650–6.
12. Larsen SB, Hanss Z, Krüger R. The genetic architecture of mitochondrial dysfunction in Parkinson's disease. Cell Tissue Res. 2018;373(1):21–37.
13. Langston JW, Ballard P, Tetrud JW, Irwin I. Chronic parkinsonism in humans due to a product of meperidine-analog synthesis. Science. 1983;219(4587):979–80.
14. Tanner CM, Kamel F, Ross GW, Hoppin JA, Goldman SM, Korell M, Marras C, Bhudhikanok GS, Kasten M, Chade AR, et al. Rotenone, Paraquat, and Parkinson's disease. Environ Health Perspect. 2011;119(6):866–72.
15. Hao C, Qu A, Xu L, Sun M, Zhang H, Xu C, Kuang H. Chiral Molecule-mediated porous Cu (x)O nanoparticle clusters with antioxidation activity for ameliorating Parkinson's disease. J Am Chem Soc. 2019;141(2):1091–9.
16. Andrabi SS, Yang J, Gao Y, Kuang Y, Labhasetwar V. Nanoparticles with antioxidant enzymes protect injured spinal cord from neuronal cell apoptosis by attenuating mitochondrial dysfunction. J Controlled Release: Official J Controlled Release Soc. 2020;317:300–11.
17. Yao Z, Zhang X, Zhao F, Wang S, Chen A, Huang B, Wang J, Li X. Ursodeoxycholic acid inhibits glioblastoma progression via Endoplasmic reticulum stress related apoptosis and synergizes with the proteasome inhibitor bortezomib. ACS Chem Neurosci. 2020;11(9):1337–46.
18. Qi H, Shen D, Jiang C, Wang H, Chang M. Ursodeoxycholic acid protects dopaminergic neurons from oxidative stress via regulating mitochondrial function, autophagy, and apoptosis in MPTP/MPP-induced Parkinson's disease. Neurosci Lett. 2021;741:135493.
19. Carling P, Mortiboys H, Green C, Mihaylov S, Sandor C, Schwartzentruber A, Taylor R, Wei W, Hastings C, Wong S, et al. Deep phenotyping of peripheral tissue facilitates mechanistic disease stratification in sporadic Parkinson's disease. Prog Neurobiol. 2020;187:101772.
20. Parry G, Rodrigues C, Aranha M, Hilbert S, Davey C, Kelkar P, Low W, Steer C. Safety, tolerability, and cerebrospinal fluid penetration of ursodeoxycholic acid in patients with amyotrophic lateral sclerosis. Clin Neuropharmacol. 2010;33(1):17–21.
21. Wu Y, Wan S, Yang S, Hu H, Zhang C, Lai J, Zhou J, Chen W, Tang X, Luo J, et al. Macrophage cell membrane-based nanoparticles: a new promising biomimetic platform for targeted delivery and treatment. J Nanobiotechnol. 2022;20(1):542.
22. Yang X, Ma Y, Xie H, Dong S, Rao G, Yang Z, Zhang J, Wu Q. Extracellular vesicles in the treatment of Parkinson's disease: A review. Curr Med Chem. 2021;28(31):6375–94.
23. Samanta S, Rajasingh S, Drosos N, Zhou Z, Dawn B, Rajasingh J. Exosomes: new molecular targets of diseases. Acta Pharmacol Sin. 2018;39(4):501–13.
24. Marrache S, Dhar S. Engineering of blended nanoparticle platform for delivery of mitochondria-acting therapeutics. Proc Natl Acad Sci U S A. 2012;109(40):16288–93.
25. Yamada Y, Harashima H. Enhancement in selective mitochondrial association by direct modification of a mitochondrial targeting signal peptide on a liposomal based nanocarrier. Mitochondrion. 2013;13(5):526–32.
26. Asayama S, Kawamura E, Nagaoka S, Kawakami H. Design of manganese porphyrin modified with mitochondrial signal peptide for a new antioxidant. Mol Pharm. 2006;3(4):468–70.
27. Neupane KR, Ramon GS, Harvey B, Chun B, Aryal SP, Masud AA, McCorkle JR, Kolesar JM, Kekenes-Huskey PM, Richards CI. Programming Cell-Derived vesicles with enhanced Immunomodulatory properties. Adv Healthc Mater 2023:e2301163.
28. Moonschi FH, Effinger AK, Zhang X, Martin WE, Fox AM, Heidary DK, DeRouchey JE, Richards CI. Cell-derived vesicles for single-molecule imaging of membrane proteins. Angew Chem Int Ed Engl. 2015;54(2):481–4.
29. Haney MJ, Klyachko NL, Zhao Y, Gupta R, Plotnikova EG, He Z, Patel T, Piroyan A, Sokolsky M, Kabanov AV, Batrakova EV. Exosomes as drug delivery vehicles for Parkinson's disease therapy. J Controlled Release: Official J Controlled Release Soc. 2015;207:18–30.

30. Zhuang X, Xiang X, Grizzle W, Sun D, Zhang S, Axtell RC, Ju S, Mu J, Zhang L, Steinman L, et al. Treatment of brain inflammatory diseases by delivering exosome encapsulated anti-inflammatory drugs from the nasal region to the brain. Mol Ther. 2011;19(10):1769–79.
31. Kim MS, Haney MJ, Zhao Y, Mahajan V, Deygen I, Klyachko NL, Inskoe E, Piroyan A, Sokolsky M, Okolie O, et al. Development of exosome-encapsulated Paclitaxel to overcome MDR in cancer cells. Nanomedicine. 2016;12(3):655–64.
32. Kim H, Wang SY, Kwak G, Yang Y, Kwon IC, Kim SH. Exosome-Guided phenotypic switch of M1 to M2 macrophages for cutaneous wound healing. Adv Sci (Weinh). 2019;6(20):1900513.
33. Rana S, Yue S, Stadel D, Zöller M. Toward tailored exosomes: the Exosomal tetraspanin web contributes to target cell selection. Int J Biochem Cell Biol. 2012;44(9):1574–84.
34. Li X, Wang S, Zhu R, Li H, Han Q, Zhao RC. Lung tumor exosomes induce a pro-inflammatory phenotype in mesenchymal stem cells via NFκB-TLR signaling pathway. J Hematol Oncol. 2016;9:42.
35. Han Y, Gao C, Wang H, Sun J, Liang M, Feng Y, Liu Q, Fu S, Cui L, Gao C, et al. Macrophage membrane-coated nanocarriers Co-Modified by RVG29 and TPP improve brain neuronal mitochondria-targeting and therapeutic efficacy in Alzheimer's disease mice. Bioactive Mater. 2021;6(2):529–42.
36. Drouin-Ouellet J. Mitochondrial complex I deficiency and Parkinson disease. Nat Rev Neurosci. 2023;24(4):193.
37. Vos M. Mitochondrial complex I deficiency: guilty in Parkinson's disease. Signal Transduct Target Ther. 2022;7(1):136.
38. Dionísio PA, Amaral JD, Rodrigues CMP. Oxidative stress and regulated cell death in Parkinson's disease. Ageing Res Rev. 2021;67:101263.
39. Cenini G, Lloret A, Cascella R. Oxidative Stress in Neurodegenerative Diseases: From a Mitochondrial Point of View. Oxidative medicine and cellular longevity 2019, 2019:2105607.
40. George PM, Steinberg GK. Novel stroke therapeutics: unraveling stroke pathophysiology and its impact on clinical treatments. Neuron. 2015;87(2):297–309.
41. Khatoon N, Zhang Z, Zhou C, Chu M. Macrophage membrane coated nanoparticles: a biomimetic approach for enhanced and targeted delivery. Biomater Sci. 2022;10(5):1193–208.
42. Wang H, Liu Y, He R, Xu D, Zang J, Weeranoppanant N, Dong H, Li Y. Cell membrane biomimetic nanoparticles for inflammation and cancer targeting in drug delivery. Biomater Sci. 2020;8(2):552–68.
43. He R, Jiang Y, Shi Y, Liang J, Zhao L. Curcumin-laden exosomes target ischemic brain tissue and alleviate cerebral ischemia-reperfusion injury by inhibiting ROS-mediated mitochondrial apoptosis. Mater Sci Eng C Mater Biol Appl. 2020;117:111314.
44. Kong DH, Kim YK, Kim MR, Jang JH, Lee S. Emerging roles of vascular cell adhesion Molecule-1 (VCAM-1) in immunological disorders and Cancer. Int J Mol Sci 2018, 19(4).
45. Li D, Xue W, Li M, Dong M, Wang J, Wang X, Li X, Chen K, Zhang W, Wu S, et al. VCAM-1(+) macrophages guide the homing of HSPCs to a vascular niche. Nature. 2018;564(7734):119–24.
46. undefined u, undefined u. Protocol for the MPTP mouse model of Parkinson's disease. Nat Protoc 2007, 2.
47. Zhou ZD, Saw WT, Ho PGH, Zhang ZW, Zeng L, Chang YY, Sun AXY, Ma DR, Wang HY, Zhou L, et al. The role of tyrosine hydroxylase-dopamine pathway in Parkinson's disease pathogenesis. Cell Mol Life Sci. 2022;79(12):599.
48. Zhou ZD, Refai FS, Xie SP, Ng SH, Chan CHS, Ho PGH, Zhang XD, Lim TM, Tan EK. Mutant PINK1 upregulates tyrosine hydroxylase and dopamine levels, leading to vulnerability of dopaminergic neurons. Free Radic Biol Med. 2014;68:220–33.
49. Wakhloo D, Oberhauser J, Madira A, Mahajani S. From cradle to grave: neurogenesis, neuroregeneration and neurodegeneration in Alzheimer's and Parkinson's diseases. Neural Regen Res. 2022;17(12):2606–14.
50. Chmielarz P, Er Ş, Konovalova J, Bandres L, Hlushchuk I, Albert K, Panhelainen A, Luk K, Airavaara M, Domanskyi A. GDNF/RET signaling pathway activation eliminates lewy body pathology in midbrain dopamine neurons. Mov Disorders: Official J Mov Disorder Soc. 2020;35(12):2279–89.
51. Meka DP, Müller-Rischart AK, Nidadavolu P, Mohammadi B, Motori E, Ponna SK, Aboutalebi H, Bassal M, Annamneedi A, Finckh B, et al. Parkin cooperates with GDNF/RET signaling to prevent dopaminergic neuron degeneration. J Clin Invest. 2015;125(5):1873–85.
52. Buitrago-Delgado E, Nordin K, Rao A, Geary L, LaBonne C. NEURODEVELOPMENT. Shared regulatory programs suggest retention of blastula-stage potential in neural crest cells. Science. 2015;348(6241):1332–5.
53. Patra M, Mahata SK, Padhan DK, Sen M. CCN6 regulates mitochondrial function. J Cell Sci. 2016;129(14):2841–51.
54. Padhan DK, Sengupta A, Patra M, Ganguly A, Mahata SK, Sen M. CCN6 regulates mitochondrial respiratory complex assembly and activity. Faseb J. 2020;34(9):12163–76.
55. Mowla SJ, Farhadi HF, Pareek S, Atwal JK, Morris SJ, Seidah NG, Murphy RA. Biosynthesis and post-translational processing of the precursor to brain-derived neurotrophic factor. J Biol Chem. 2001;276(16):12660–6.
56. Mizui T, Ishikawa Y, Kumanogoh H, Kojima M. Neurobiological actions by three distinct subtypes of brain-derived neurotrophic factor: Multi-ligand model of growth factor signaling. Pharmacol Res. 2016;105:93–8.
57. Dehay B, Bourdenx M, Gorry P, Przedborski S, Vila M, Hunot S, Singleton A, Olanow CW, Merchant KM, Bezard E, et al. Targeting α-synuclein for treatment of Parkinson's disease: mechanistic and therapeutic considerations. Lancet Neurol. 2015;14(8):855–66.
58. Devine MJ, Gwinn K, Singleton A, Hardy J. Parkinson's disease and α-synuclein expression. Mov Disorders: Official J Mov Disorder Soc. 2011;26(12):2160–8.
59. Syringas M, Janin F, Mezghanni S, Giros B, Costentin J, Bonnet JJ. Structural domains of chimeric dopamine-noradrenaline human transporters involved in the Na(+)- and Cl(-)-dependence of dopamine transport. Mol Pharmacol. 2000;58(6):1404–11.
60. Giros B, el Mestikawy S, Godinot N, Zheng K, Han H, Yang-Feng T, Caron MG. Cloning, Pharmacological characterization, and chromosome assignment of the human dopamine transporter. Mol Pharmacol. 1992;42(3):383–90.
61. Bademci G, Edwards TL, Torres AL, Scott WK, Züchner S, Martin ER, Vance JM, Wang L. A rare novel deletion of the tyrosine hydroxylase gene in Parkinson disease. Hum Mutat. 2010;31(10):E1767–1771.
62. Kooshki L, Zarneshan SN, Fakhri S, Moradi SZ, Echeverria J. The pivotal role of JAK/STAT and IRS/PI3K signaling pathways in neurodegenerative diseases: mechanistic approaches to polyphenols and alkaloids. Phytomedicine. 2023;112:154686.
63. Qin H, Buckley JA, Li X, Liu Y, Fox TH 3rd, Meares GP, Yu H, Yan Z, Harms AS, Li Y, et al. Inhibition of the JAK/STAT pathway protects against α-Synuclein-Induced neuroinflammation and dopaminergic neurodegeneration. J Neurosci. 2016;36(18):5144–59.
64. Wegrzyn J, Potla R, Chwae YJ, Sepuri NB, Zhang Q, Koeck T, Derecka M, Szczepanek K, Szelag M, Gornicka A, et al. Function of mitochondrial Stat3 in cellular respiration. Science. 2009;323(5915):793–7.
65. Lashgari NA, Khayatan D, Roudsari NM, Momtaz S, Dehpour AR, Abdolghaffari AH. Therapeutic approaches for cholestatic liver diseases: the role of nitric oxide pathway. Naunyn Schmiedebergs Arch Pharmacol. 2024;397(3):1433–54.
66. Hong H, Wang Y, Menard M, Buckley JA, Zhou L, Volpicelli-Daley L, Standaert DG, Qin H, Benveniste EN. Suppression of the JAK/STAT pathway inhibits neuroinflammation in the line 61-PFF mouse model of Parkinson's disease. J Neuroinflammation. 2024;21(1):216.
67. Hibino M, Maeki M, Tokeshi M, Ishitsuka Y, Harashima H, Yamada Y. A system that delivers an antioxidant to mitochondria for the treatment of drug-induced liver injury. Sci Rep. 2023;13(1):6961.
68. Shen Y, Liang L, Zhang S, Huang D, Zhang J, Xu S, Liang C, Xu W. Organelle-targeting surface-enhanced Raman scattering (SERS) nanosensors for subcellular pH sensing. Nanoscale. 2018;10(4):1622–30.
69. Wang J, Ma X, Wu Z, Cui B, Zou C, Zhang P, Yao S. Microfluidics-Prepared Ultrasmall biomimetic nanovesicles for brain tumor targeting. Adv Healthc Mater. 2024;13(5):e2302302.
70. Liu P, Wang S, Wang G, Zhao M, Du F, Li K, Wang L, Wu H, Chen J, Yang Y, Su G. Macrophage-derived Exosomal miR-4532 promotes endothelial cells injury by targeting SP1 and NF-κB P65 signalling activation. J Cell Mol Med. 2022;26(20):5165–80.
71. Wen Y, Fu Q, Soliwoda A, Zhang S, Zheng M, Mao W, Wan Y. Cell-derived nanovesicles prepared by membrane extrusion are good substitutes for natural extracellular vesicles. Extracell Vesicle 2022, 1.
72. Wan Y, Cheng G, Liu X, Hao SJ, Nisic M, Zhu CD, Xia YQ, Li WQ, Wang ZG, Zhang WL et al. Rapid magnetic isolation of extracellular vesicles via lipid-based nanoprobes. Nat Biomed Eng 2017, 1.
73. Ilahibaks NF, Lei Z, Mol EA, Deshantri AK, Jiang L, Schiffelers RM, Vader P, Sluijter JPG. Biofabrication of Cell-Derived Nanovesicles: A Potential Alternative to Extracellular Vesicles for Regenerative Medicine. Cells 2019, 8(12).
74. Ekmekcioglu A, Gok O, Oz-Arslan D, Erdal MS, Yagan Uzuner Y, Muftuoglu M. Mitochondria-Targeted liposomes for drug delivery to tumor mitochondria. Pharmaceutics 2024, 16(7).

75. Li XY, Zhu SH, Yang F, Hu GX, Yuan LJ. An ultra-performance liquid chromatography-tandem mass spectrometry method for the determination of obeticholic acid in rat plasma and its application in preclinical Pharmacokinetic studies. J Chromatogr B Analyt Technol Biomed Life Sci. 2019;1121:82–8.
76. Ilyasov IR, Beloborodov VL, Selivanova IA, Terekhov RP. ABTS/PP decolorization assay of antioxidant capacity reaction pathways. Int J Mol Sci 2020, 21(3).
77. Jackson-Lewis V, Przedborski S. Protocol for the MPTP mouse model of Parkinson's disease. Nat Protoc. 2007;2(1):141–51.
78. Khalaf K, Tornese P, Cocco A, Albanese A. Tauroursodeoxycholic acid: a potential therapeutic tool in neurodegenerative diseases. Transl Neurodegener. 2022;11(1):33.
79. Huang F, Pariante CM, Borsini A. From dried bear bile to molecular investigation: A systematic review of the effect of bile acids on cell apoptosis, oxidative stress and inflammation in the brain, across pre-clinical models of neurological, neurodegenerative and neuropsychiatric disorders. Brain Behav Immun. 2022;99:132–46.
80. Bhalerao A, Sivandzade F, Archie SR, Chowdhury EA, Noorani B, Cucullo L. In vitro modeling of the neurovascular unit: advances in the field. Fluids Barriers CNS. 2020;17(1):22.
81. Omidi Y, Campbell L, Barar J, Connell D, Akhtar S, Gumbleton M. Evaluation of the immortalised mouse brain capillary endothelial cell line, b.End3, as an in vitro blood-brain barrier model for drug uptake and transport studies. Brain Res. 2003;990(1–2):95–112.
82. Brown RC, Morris AP, O'Neil RG. Tight junction protein expression and barrier properties of immortalized mouse brain microvessel endothelial cells. Brain Res. 2007;1130(1):17–30.
83. Cao Q, Qin L, Huang F, Wang X, Yang L, Shi H, Wu H, Zhang B, Chen Z, Wu X. Amentoflavone protects dopaminergic neurons in MPTP-induced Parkinson's disease model mice through PI3K/Akt and ERK signaling pathways. Toxicol Appl Pharmacol. 2017;319:80–90.
84. Li HY, Liu DS, Li LB, Zhang YB, Dong HY, Rong H, Zhang JY, Wang JP, Jin M, Luo N, Zhang XJ. Total glucosides of white Paeony capsule ameliorates Parkinson's disease-like behavior in MPTP-induced mice model by regulating LRRK2/alpha-synuclein signaling. J Ethnopharmacol. 2024;319(Pt 2):117319.
85. Wang W, Shi L, Xie Y, Ma C, Li W, Su X, Huang S, Chen R, Zhu Z, Mao Z, et al. SP600125, a new JNK inhibitor, protects dopaminergic neurons in the MPTP model of Parkinson's disease. Neurosci Res. 2004;48(2):195–202.
86. Chen S, Zhou Y, Chen Y, Gu J. Fastp: an ultra-fast all-in-one FASTQ preprocessor. Bioinformatics. 2018;34(17):i884–90.
87. Kim D, Langmead B, Salzberg SL. HISAT: a fast spliced aligner with low memory requirements. Nat Methods. 2015;12(4):357–60.
88. Anders S, Pyl PT, Huber W. HTSeq–a Python framework to work with high-throughput sequencing data. Bioinformatics. 2015;31(2):166–9.
89. Love MI, Huber W, Anders S. Moderated Estimation of fold change and dispersion for RNA-seq data with DESeq2. Genome Biol. 2014;15(12):550.

Publisher's note

Springer Nature remains neutral with regard to jurisdictional claims in published maps and institutional affiliations.